TOPICAL REVIEW

Optically and thermally induced molecular switching processes at metal surfaces

Petra Tegeder

Freie Universität Berlin, Fachbereich Physik, Arnimallee 14, D-14195 Berlin, Germany

E-mail: petra.tegeder@physik.fu-berlin.de

Abstract. Using light to control the switching of functional properties of surface-bound species is an attractive strategy for the development of new technologies with possible applications in molecular electronics and functional surfaces and interfaces. Molecular switches are promising systems for such a route since they possess the ability to undergo reversible changes between different molecular states and accordingly molecular properties by excitation with light or other external stimuli. In this review, recent experiments on photo- and thermally induced molecular switching processes at nobel metal surfaces utilizing two-photon photoemission and surface vibrational spectroscopies are reported. The investigated molecular switches can either undergo a *trans/cis*-isomerization or a ring-opening/closure reaction. Two approaches concerning the connection of the switches to the surface are applied; physisorbed switches, i.e., molecules in direct contact with the substrate and surface-decoupled switches incorporated in self-assembled monolayers. Elementary processes in molecular switches at surfaces such as excitation mechanisms in the photoisomerization and kinetic parameters for thermally driven reactions, are presented, which are essential for a microscopic understanding of molecular switching at surfaces. This in turn is needed for designing an appropriate adsorbate/substate system with the desired switchable functionality controlled by external stimuli.

Submitted to: *J. Phys.: Condens. Matter*

1. Introduction

The switching of functional molecular properties *via* conformational changes is a fundamental concept in nature. In many biological systems the specific functions are based on the cooperation of individual molecular units which are enabled and controlled by defined changes in the molecular geometry. A prominent example is the light-induced *cis*- to *trans*-isomerization of retinal, which plays a key role in the vision process [1]. Such switching processes represent an attractive strategy for the development of new technologies. The possibility to design molecules with specific functional properties opens the perspective to use molecules as building blocks for integrated functional devices [2, 3]. However, for possible applications in the field of

molecular electronics and functional surfaces [3, 4, 5, 6, 7, 8, 9, 10, 11] it is essential to control the switching between different stable (or metastable) molecular states and to connect the molecular system to (metal) electrodes. This requires an understanding of structural and electronic properties including the interaction with solid interfaces and the control of the switching between different molecular conformations by external stimulation for instance electromagnetic fields.

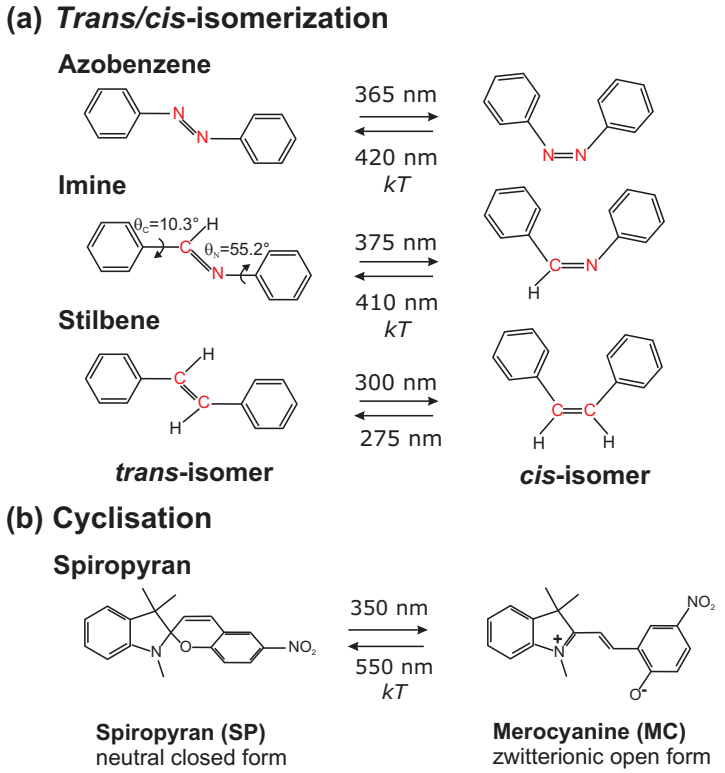

Figure 1. Photochromic systems: (a) Azobenzene, imine, and stilbene undergo a reversible photoinduced *trans/cis*-isomerization and (b) spiropyran performs a reversible photoinduced ring-opening/-closing reaction and a thermally activated ring closure reaction.

Photochromic molecular switches permit the control of molecular geometry and functional properties *via* excitation with light at appropriate wavelengths [12, 13, 14, 15, 16, 17]. Thereby the molecules are interconverted reversibly between at least two (meta)-stable states as a result of a *trans/cis*-isomerization like in azobenzene, (see Fig. 1(a)), a photocyclisation like in spiropyran (see Fig. 1(b)) or a combination of both. Derivatives of the molecular switches shown in Fig. 1 have been investigated in the present study. In the case of azobenzenes and imines a thermally activated *cis* $\rightarrow$ *trans* reaction is possible besides the photoinduced isomerization (see Fig.3(a)). In contrast, for stilbene and its derivatives the thermal back reaction is unlikely since the activation barrier (E_a) is in the order of 1.9 eV [18, 19, 20] thus much higher compared to azobenzenes ($E_a \approx$ 1eV [21, 22, 23]) and imines ($E_a \approx 0.7$ eV [24, 25]). In the electronic ground state the *trans*-isomer of azobenzene, stilbene, and imine is lower in energy com-

pared to the *cis*-isomer and the *trans*-form is planar except for imine, which adopts a three-dimensional (3D) structure. Spiropyran (SP) in its closed-form is 3D, while the open isomer (merocyanine, MC) is planar and existent in a zwitterionic-form, hence it exhibits a large dipole moment. For spiropyran the ring-closing reaction can also be driven by thermal activation.

Adsorbate/substrate-interaction

Whereas the switching properties of the free molecules in solution are well-understood, it is a key questions how these are changing when the molecules are bound to a (metallic) substrate. Thereby the significant parameter is the strength of the molecule/substrate-interaction which determines the adsorption geometry as well as the electronic structure of the adsorbate. Two different concepts concerning the connection of the molecular switches to the surface can be traced (see Fig. 2):
(i) physisorbed or weakly chemisorbed systems (horizontal adsorption geometry) and
(ii) *via* anchoring groups covalently attached molecular switches incorporated in a self-assembled monolayer (SAM; vertical adsorption geometry).

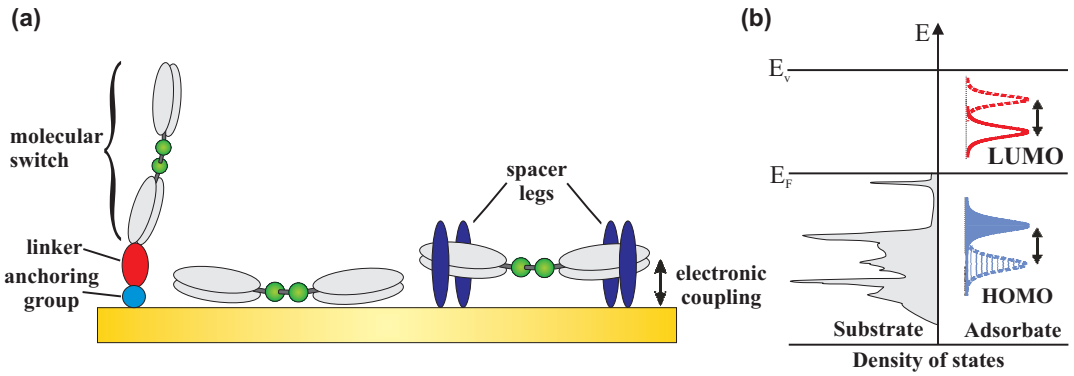

Figure 2. (a) Adsorption of molecular switches *via* an anchoring group, leading to a vertical orientation and physisorbed systems in which the molecules are in direct contact with the substrate. Spacer groups yield to a reduced electronic coupling between the molecules and the substrate. (b) Dependency of the energetic positions of occupied and unoccupied molecular states on the electronic coupling strength.

While in the first case the switches are directly bound to the substrate, in the second case the distance and thus the electronic coupling between the molecules and the surface depends on the anchor/linker-system. By varying the length and the composition (e.g. alkyl or unsaturated carbon chains) of the linker the coupling can be changed. In order to reduce the electronic coupling of the physisorbed molecules bulky substituents, for instance *tert*-butyl- or di-methyl-phenyl-groups which act as "spacer-legs" can be used [26, 27]. The electronic coupling strength plays an important role since it determines the energetic positions of occupied (e.g., the highest occupied molecular orbital, HOMO) and unoccupied molecular orbitals (e.g., the lowest unoccupied molecular orbital, LUMO) and the lifetime of molecular excited states. At metal surfaces the lifetime of molecular excited states will decrease strongly compared to the one for molecules in the gas or

liquid phase [28]. Thus, their switching properties are presumably not preserved at surfaces and rather different isomerization mechanisms may be accessible.

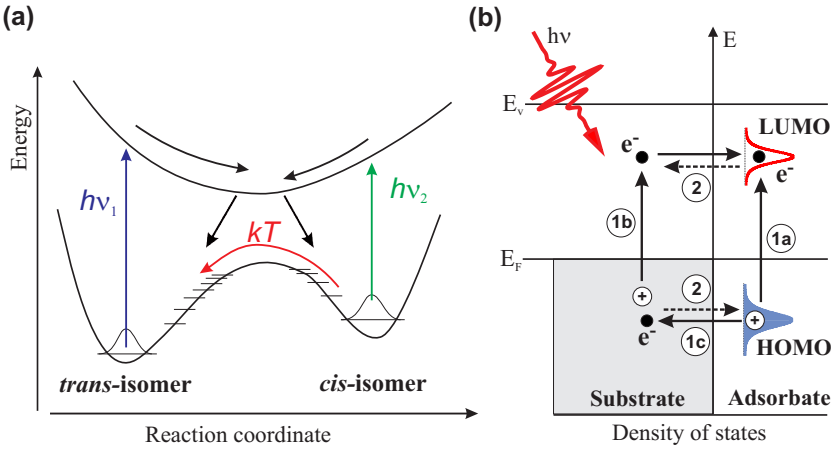

Figure 3. (a) Scheme of the reversible *trans*/*cis*-isomerization induced by light at appropriate wavelengths and the thermal activated *cis* → *trans* reaction for molecular switches in the liquid or gas phase (for simplicity only one excited state is shown). (b) Possible excitation mechanisms in the photoisomerization of molecular switches at metal surfaces: 1a) Intramolecular electronic excitation, 1b) formation of a negative ion resonance *via* attachment of hot electrons, 1c) creation of a positive ion resonance through hole transfer to an occupied molecular state and 2) decay of the resonance by back-transfer of the electron or hole to the substrate.

Figure 3 (b) shows schematically possible photoinduced excitation mechanisms of molecular switching at surfaces: 1a) The direct (intramolecular) electronic excitation (HOMO-LUMO transition) analogous to the isomerization in solution. 1b) A photoinduced charge transfer between the substrate and adsorbate, leading to the formation of a negative ion resonance. Such substrate-mediated photochemical reactions where hot electrons induce a chemical process on metal surfaces like desorption and dissociation have been discussed for various systems [29, 30, 31, 32, 33, 34]. 1c) The formation of a positive ion resonance *via* a hole transfer from the metal substrate to the adsorbate. Hot hole stimulated processes are well-known from photochemistry of adsorbates on semiconductor surfaces [31, 35, 36, 37, 38, 39]. The molecular excited states generated by all pathways (1a, 1b and 1c) will decay *via* back-transfer of the electron or hole to the substrate (channel 2 in Fig. 3(b)). However, at metal surfaces the lifetimes of excited states are expected to be ultrashort, i.e., in the range of femtoseconds as shown for different adsorbates [40, 41, 42, 43, 44]. This competition between the required nuclear motion and quenching of excited states provides a challenge to realize photoinduced molecular switching at metal surfaces.

The influence of the adsorbate/substrate-interaction on the photoisomerization probability has been demonstrated by Crommie *et al.* [45] in the case of azobenzene derivatives bound to a Au(111) surface using scanning tunneling microscopy (STM). In this study, the parent (unsubstituted) azobenzene and azobenzene functionalized with *tert*-butyl-groups acting as "spacer-legs" (see above), namely two spacer legs, one

on each phenyl ring (4,4‘-di-*tert*-butyl-azobenzene (DBA)) and four spacer legs, two on each phenyl ring (3,3‘,5,5‘-tetra-*tert*-butyl-azobenzene (TBA)) adsorbed on Au(111) have been investigated. STM images of the azobenzenes reveal the differences between adsorbed bare azobenzene, DBA, and TBA. Bare azobenzene molecules appear as pairs of closely touching lobes, with each lobe indicating the position of a single phenyl ring. Individual DBA molecules similarly appear as a pair of lobes, except that the DBA lobes are separated by a wider distance. Individual TBA molecules appear as four-lobed structures. Thereby the appearance of DBA and TBA is consistent with their expected *tert*-butyl-groups arrangements. Constant-current line scans across the azobenzene derivatives show that the DBA and TBA molecules are progressively taller than bare azobenzene molecules. Hence, the use of *tert*-butyl-groups results in an increase of the adsorbate-surface distance (see chapter 3.3). Illumination with UV-light of the different azobenzenes on Au(111) revealed that only the TBA molecules undergo a photoisomerization presumably due to a reduced coupling, demonstrating the influence of the adsorbate/substrate-interaction on the isomerization properties.

Adsorbate/adsorbate-interaction

Beside the adsorbate/substrate-interaction, in a molecular ensemble lateral adsorbate/adsorbate-interactions exert influence on the switching process. It has been shown for an azobenzene derivative, the 4-methoxy-3,3‘,5,5‘-tetra-*tert*-butyl-azobenzene (M-TBA) adsorbed on Au(111) that the switching capability of each individual molecule depends on both the surrounding molecules and the underlying surface structure [46]. Thereby the dimensions and the orientation of the ”switching lattice” neither reflect the Au(111) lattice nor the herringbone reconstruction. It can only be explained in terms of commensurability between the molecular layer and the underlying substrate. A similar effect has been observed for the TBA adsorbed on Au(111) [47].

In SAMs functionalized with molecular switches, for example azobenzenes, space is required (free volume) to allow the conformational change since the *trans/cis*-isomerization is associated with a significant structural change. In a densely packed and highly ordered film, for instance in azobenzene-substituted alkanethiols on gold, the free volume needed for the isomerization is limited and therefore the photoinduced switching is restricted due to steric hinderance. However for highly ordered films of aromatic azobenzene-biphenyls (4‘-(biphenyl-4-ylazo)biphenyl-4-thio) adsorbed on Au and Pt cooperative light-induced transformation of whole domains has been observed [48, 49]. Different approaches have been attempted to overcome the problem of steric hinderance. For example photoinduced switching has been obtained in mixed SAMs where azobenzene-containing molecules were isolated in a matrix of short alkanethiols [50, 51]. However this strategy may lead to phase separation of the two components within the film and to aggregation of the azobenzene-bearing molecules due to π-stacking of the aromatic units. Accordingly the photoisomerization is restricted to adsorbed molecules at the domain boundaries. Another route is to use lateral spacers, e.g., para-carborane in the alkyl chain [52] or a host-guest inclusion complex between

α-cyclodextrin and an azobenzene-terminated alkanethiol [53], which yielded a high photoisomerization capacity. In addition adsorbates with two anchoring groups, bound *via* short alkyl chains have been investigated but no improved switching was observed [54]. An alternative approach is to attach the molecular switches to a metal surface *via* customizable molecular platforms with a defined adsorption geometry. These platforms act as pedestals that enforce a controlled orientation of the molecular switch relative to the surface and determine by their size the spacing between the switches [55, 56].

Among the free volume needed for the isomerization, it has been shown for a highly ordered azobenzene-functionalized SAM with a dense packed photochrome that excitonic coupling may lead to an ultrafast lateral delocalization of the optical excitation, *viz.* the intermolecular interaction results in a suppression of the isomerization process [57, 58].

While several studies on light induced isomerization of molecular switches incorporated in SAMs are existing [59], investigations on the photoisomerization of switches directly bound to a metallic substrate are limited [11, 60] and have been demonstrated so far only for a specifically designed azobenzene derivative, namely TBA adsorbed on Au(111) [61, 45, 62]. Beside the stimulation with light the STM-tip has been applied in particular to induce reversible conformational changes [63]. Thereby *trans/cis*-isomerizations have been achieved by resonant [64] and inelastic [65, 66] tunneling and *via* the applied electric field [67, 68, 46].

Molecular switches at surfaces: potential applications

Studies on physisorbed molecular switches directly bound to the substrate provide detailed insights into elementary processes in molecular switches at surfaces such as excitation mechanisms in the photoisomerization and kinetic parameters for thermally driven reactions, however, from a applied standpoint the practical use of such functionalized surfaces is rather limited. In contrast molecular switches incorporated in SAMs covalently attached (chemisorbed) to the substrate promise a much higher potential for the generation of (photo)switchable surfaces [59, 69, 70, 71, 72]. A switching ability opens the opportunity to create functional surfaces with properties, for instance electronic, wetting, (electronic) transport or non-linear optical properties which can be switched at will.

For instance, it has demonstrated that an azobenzene functionalized flat gold surface is capable to control the cell adhesion [73]. Thereby the azobenzene is substituted with a ariginine-glycine-aspartate (RGD) enabling cell adhesion when azobenzene adopts its *trans*-configuration. Illumination with UV light leads to largely reduced cell adhesion as the RGD unit becomes less accessible due to the *trans* to *cis* isomerization of the azobenzene moiety. Light exposure in the visible range (*cis* to *trans* isomerization) resulted in the reverse process, i.e., enhanced cell adhesion. This dynamic control of cell adhesion is significant for many biological applications, e.g. cell migration. Converting light energy into mechanical work has been shown in an photoswitchable azobenzene containing SAM in an electrical metal-molecule-metal junction, in which a

Hg drop was lifted upon *trans* → *cis*-isomerization [49]. Using photo-switchable SAMs attached to curved surfaces, namely Au-nanoparticles (NP) facilitated optically induced isomerization accompanied by reversible NP aggregation [74]. The ability to reversible self-assemble NP using light combined with the fact that the aggregation process comes along with pronounced color changes may allow to develop novel rewritable information storage media, in which writing and erasing can be controlled by light [75].

The present review

In this work we employed two-photon photoemission (2PPE) spectroscopy to gain insights into the electronic structure, i.e., occupied and unoccupied electronic states of molecular switches adsorbed on noble metal surfaces. A detailed knowledge about the electronic structure of the molecules in contact with metal substrates is a key issue in order to elucidate the excitation mechanism for the photostimulated isomerization. 2PPE has been used in various adsorbate-substrate systems to study adsorbate and image potential states [76, 77, 78, 79, 80, 81, 82, 83]. Moreover, 2PPE can be carried out in a time-resolved fashion for the determination of electron dynamics on a femtosecond time scale [77, 84]. In addition, high resolution electron energy loss spectroscopy (HREELS) and sum-frequency generation (SFG) vibrational spectroscopy are applied to study the adsorption geometry (molecular orientation) of the switchable molecules. Angular-dependent HREELS measurements permit to separate dipole- and impact-scattering components thus allowing to analyze the geometrical structure and predominantly the orientation of functional groups with respect to the metallic substrate [85]. SFG is a well known nonlinear optical technique for studying interfaces. These studies range from interfaces of liquids, SAMs on metal surfaces, electrochemical and catalytic reactions to dynamics and kinetics at interfaces in consequence of the temporal resolution of SFG [86, 87, 88, 89, 90, 91, 92, 93, 94, 95, 96]. It is surface-selective due to the fact that, as a second-order process in the dielectric field, it is forbidden under the electric-dipole approximation in a medium with centrosymmetry. At a surface or interface the inversion symmetry is broken. Due to the unique symmetry selection rule of the second-order nonlinear optical process, this technique is intrinsically surface-sensitive, in contrast to infrared and Raman spectroscopies. As we will demonstrate all three experimental techniques allow to analyze photoinduced and thermally activated isomerization processes since these processes are associated with changes in the electronic and geometrical structure of the molecular switches.

We studied the switching (*trans/cis*-isomerization) properties of surface-bound azobenzene, imine, and stilbene derivatives (see Fig. 1 (a)) all functionalized with tetra-*tert*-butyl-groups, which are believed to act as spacer groups to reduce the electronic coupling between the photochemically active group and the metallic substrate (Au(111) or Ag(111)). We discuss the role of *tert*-butyl spacer legs on the basis of precise measurements of the molecular adsorption geometries for azobenzenes using the normal incidence X-ray standing wave technique (NIXSW) and corresponding large-scale density-functional theory (DFT) calculations. In addition, the photo- and STM-induced

and thermally activated isomerization ability of trimethyl-6-nitro-spiropyran adsorbed on Au(111), which undergoes a ring-opening/ring-closure reaction in the liquid phase (see Fig. 1 (b)), is investigated. Furthermore, an example for the photoisomerization of an azobenzene-functionalized SAM immobilized on a gold surface will be given.

This review is organized as follows: Chapter 2 provides an overview over the experimental methods applied to obtain information on optically and thermally induced isomerization processes at surfaces. In Chapter 3 the main results on the *trans/cis*-isomerization studies are presented and discussed. In Section 4 we introduce and discuss the findings for spiropyran derivative adsorbed on Au(111). In Section 5 we consider the photoisomerization study of azobenzene incorporated in a SAM. Finally, a conclusion and an outlook will be given.

2. Experimental Methods

In order to study photoinduced and thermally activated isomerization processes of molecular switches at surfaces two-photon photoemission (2PPE), high resolution electron energy loss spectroscopy (HREELS), and sum-frequency generation (SFG) vibrational spectroscopy are used. 2PPE provides insights into the electronic structure, i.e., occupied and unoccupied states of the adsorbate/substrate-system. Thereby reversible changes in the electronic structure allow to gain mechanistic and quantitative insight into the switching process. HREELS and SFG are employed to analyze the adsorption geometry (molecular orientation) of the molecular switches and to verify isomerization reactions *via* changes in the geometrical structure. While HREELS is utilized to study physisorbed systems ("horizontal" adsorption geometry), SFG is employed for SAMs ("vertical" adsorption geometry). Several excellent overview articles exist describing in detail the basic principles and the potential of the experimental methods used in this work (2PPE: [97, 84, 76, 77, 78]; HREELS: [85, 98]; SFG: [86, 87, 88, 89, 90, 91]). Therefore only a brief review over the experimental techniques will be given. In addition the preparation procedures of the adsorbate-covered surfaces and the coverage quantification will be described.

2.1. Two-photon photoemission spectroscopy

The 2PPE experimental setup combines a tunable femtosecond laser system with an ultrahigh vacuum (UHV) chamber for photoemission spectroscopy and surface science techniques. The latter includes low energy electron diffraction (LEED) and thermal desorption spectroscopy (TDS).

For the 2PPE measurements, femtosecond laser pulses are generated by a 300 kHz Ti:Sapphire laser system which pumps an optical parametric amplifier (OPA) (see Fig. 4 (a)). The OPA 9450 (visible optical parametric amplifier (VIS-OPA)) delivers tunable VIS pulses (460–760 nm, 55 fs at 150 nJ/pulse); the OPA 9850 (infrared optical parametric amplifier (IR-OPA)) generates ultrashort infrared pulses (1100–1600 nm, 30

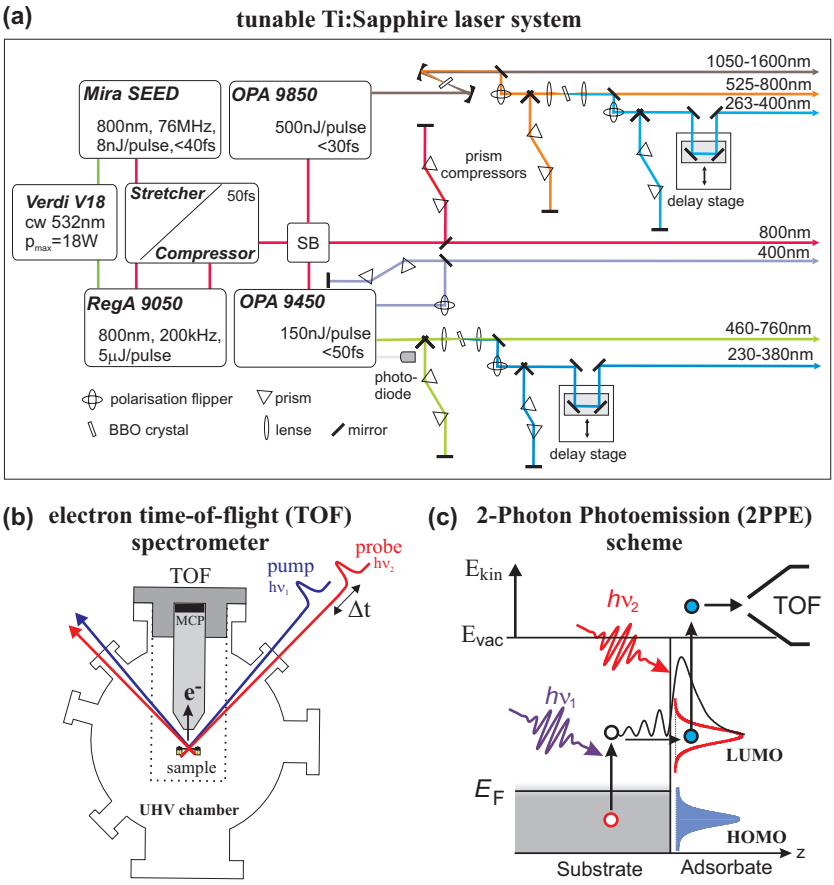

Figure 4. Schematic experimental setup for two-photon photoemission. (a) To achieve a wide tunability of femtosecond laser pulses, a regeneratively amplified (RegA) laser system operating at 200–300 kHz has been used. Its output drives two optical parametric amplifiers (OPAs) which generate a signal output in the VIS or IR range. Frequency doubling or quadrupling of the OPA and RegA laser pulses cover a wide spectral range as indicated. (b) Pairs of laser pulses at well-chosen photon energy which can be time-delayed with respect to each other are focussed onto the surface in the UHV chamber. The kinetic energy of photoelectrons is analyzed by a electron time-of-flight (TOF) spectrometer. (c) Scheme of the 2PPE process: A pump pulse $h\nu_1$ excites an electron from below the Fermi level (E_F) to intermediate unoccupied states, e.g. the lowest unoccupied molecular orbital (LUMO) at energies $E - E_F = E_{kin} + \Phi - h\nu_2$, (with Φ the work function), the probe pulse $h\nu_2$ photoionizes the sample by lifting the excited electron above the vacuum level (E_{vac}).

fs at 500 nJ/pulse). The range of photon energies is then further extended into the UV by second harmonic generation (SHG) in β-barium-borate (BBO) crystals. Frequency doubling of the VIS-OPA output yields 230–380 nm (5.4–3.3 eV). The laser pulses are incident on the surface with an angle of 45° with respect to the surface normal (see Fig. 4 (b)). While the pump pulse $h\nu_1$ excites an electron from below the Fermi level E_F to intermediate unoccupied states, e.g. the lowest unoccupied molecular orbital (LUMO) at energies $E - E_F = E_{kin} + \Phi - h\nu_2$, (with Φ the work function), the probe pulse $h\nu_2$ photoionizes the sample by lifting the excited electron above the vacuum

level (E_{vac}) (see Fig. 4 (c)). Note that for the 2PPE experiments it is necessary to avoid direct photoemission and adapt the maximum photon energy to the sample work function. Applying a time delay between the pump and the probe pulse allows to follow the temporal evolution of excited states, i.e., for instance the lifetime of a negative ion resonance. As schematically shown in Figure 4(b) photoelectrons are detected in an electron time-of-flight (TOF) spectrometer and analyzed with respect to their kinetic energy E_{kin}. The energy resolution of the TOF spectrometer depends on the electron energy, it is $\approx$ 20 meV at $E_{kin} \approx 1$ eV.

Variation of the electron detection angle α with respect to the surface normal allows to determine the electron momentum parallel to the surface $\hbar k_{||}$ according to

$$\hbar k_{||} = \sqrt{2m_e E_{kin}} \cdot \sin\alpha \tag{1}$$

where m_e denotes the free electron mass. $k_{||} = 0$ corresponds to electrons detected along the surface normal ($\alpha = 0$). For dispersion measurements, the vacuum levels of the sample and spectrometer have to be balanced due to their different work functions by applying an appropriate bias voltage to the sample. Thereby, deformation of the angular distribution of the emitted electrons by electric fields is minimized.

In order to identify whether photoemission peaks originate from occupied initial states, unoccupied intermediate states, or unoccupied final states in the 2PPE process, their dependence on photon energy is investigated. When an unoccupied state, such as the LUMO, is probed in one-color 2PPE the absorption of the first photon excites an electron from occupied orbitals to an unoccupied intermediate state; the absorption of a second photon excites this transient electron above the vacuum level. In this case, the change in electron kinetic energy scales with that in photon energy ($h\nu$ and $h\nu'$), i.e., $\Delta E_{kin} = 1\Delta h\nu$ ($\Delta h\nu = h\nu - h\nu'$). On the other hand, for two-photon nonresonant excitation from an occupied state, e.g., the highest occupied molecular orbital (HOMO), the kinetic energy of the electron ejected scales with twice the photon energy, i.e., $\Delta E_{kin} = 2\Delta h\nu$. 2PPE can also probe an unoccupied state above the vacuum level (unoccupied final states), where E_{kin} is independent of photon energy ($\Delta E_{kin} = 0\Delta h\nu$). This can be viewed as a resonant scattering event in which the photoexcited electron resides transiently in the molecular resonance, followed by detachment and detection. This analysis is generally not applicable for transitions between bulk bands due to their strong dispersion perpendicular to the surface, it holds in case of surface states and adsorbate-induced states [99, 100].

The 2PPE spectra presented below are displayed as 2PPE intensity versus the final state energy with respect to the Fermi level ($E_F = 0$ eV), $E_{final} - E_F = E_{kin} + \Phi$. In this representation one preserves the energy of an unoccupied intermediate state by subtracting the photon energy of the probe pulse $h\nu_{1or2}$ [101]. In the case of occupied initial states the photon energies of both the pump and probe pulse have to be subtracted in order to achieve the energetic position of the electronic state.

Photoisomerization experiments: For the photoinduced switching excitation by fs-laser pulses with photon energies ranging from 1.7 to 4.8 eV were used. Since in

the case of tetra-*tert*-butyl-azobenzene (TBA) adsorbed on Au(111) exposure to UV- and visible-photons induces changes in the 2PPE features due to isomerization, 2PPE spectra were recorded for 5 s only. This corresponds to a light exposure of less than 1% of exposure required to reach the photostationary state (PSS), i.e., the photoinduced changes are negligible.

2.2. High resolution electron energy loss spectroscopy

The HREELS experiments were performed in an UHV apparatus consisting of two chambers separated by a gate valve. The upper chamber was used for sample preparation and contained facilities for LEED, TDS, deposition of the molecules, and surface cleaning by noble gas ion sputtering. The lower chamber houses a high resolution electron energy loss (HREEL) spectrometer for recording vibrational spectra.

The HREEL spectrometer (Ibach-type) consists of two sub-systems the electron monochromator and analyzer, both with double-pass 127° cylindrical deflectors [98] (see Fig. 5). A monochromatic electron beam (primary energy usually about 1-10 eV)

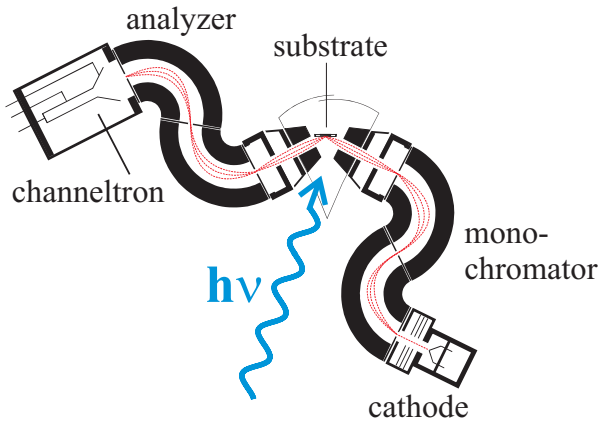

Figure 5. Scheme of the experimental setup for high resolution electron energy loss spectroscopy (HREELS). The arrangement allows illumination of the sample and carrying out HREELS without changing the sample position.

is directed onto a surface, and the energy distribution of the scattered beam is measured, eventually as a function of the primary energy, angle of incidence or scattering. The electrons in this energy range can effectively excite vibrations of surface atoms or adsorbates. In comparison to infrared (IR) spectroscopy which is as well capable to probe vibrations of adsorbed species, HREELS allows to investigate low-frequency modes ($<$ 500 cm^{-1}) which are not accessible by conventional Fourier-transform IR spectrometers. In contrast to IR spectroscopy of adsorbates at metal surfaces, in which only a dipole excitation mechanism is operative [102, 103], HREELS comprise dipole, impact and resonance scattering [85].

The *dipole scattering* is the most important excitation mechanism for adsorbates in HREELS. It results from the long-range interaction between the electric field of the incoming electron with the dynamic dipole of the adsorbate or surface (see Fig. 6 (a)).

Due to the screening of a dipole on a metal surface, there is a selection rule for dipole scattering, i.e., only vibrations with a component of the dipole moment change normal to the surface are observable. As shown in Figure 6(b) a dipole on a metal surface induces an image dipole within the substrate. Thereby the perpendicular component is doubled, whereas the parallel component is canceled by its instantaneous image. The inelastic dipole scattering involves little momentum transfer and thus the angular distribution of inelastically scattered electrons is close to the specular direction ($\theta_i = \theta_r$) (see Fig. 6 (c))

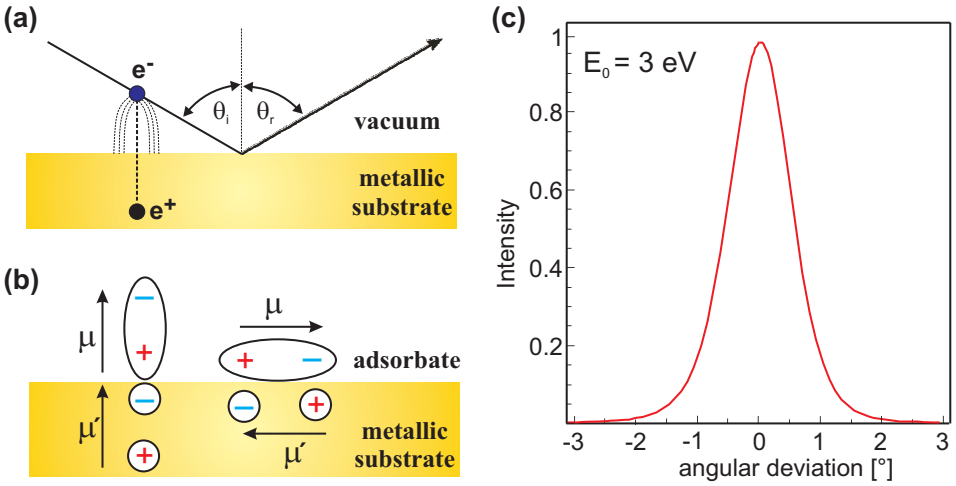

Figure 6. Schematic representation of the dipole scattering: (a) Generation of an electric field due to the approach of an electron in front of a metallic substrate. (b) Qualitative explanation of the orientation selection rule for dipole surface scattering: the image dipole within the substrate compensates the effect of the adsorbed dipole for parallel orientation but enhances the effect of dipoles with a normal orientation. (c) Intensity of dipole scattered electrons with a primary electron energy of ≈ 3 eV as a function of angular derivation with respect to the specular position.

The *impact scattering* is a short-range (few Å) direct Coulomb interaction between the incident electron and the ion cores of the adsorbate. The momentum transfer *via* this mechanism is strong therefore scattered electrons are not concentrated in the specular direction in contrast to dipole scattering. The cross section of impact scattering is about 2–3 orders of magnitude lower than that of dipole scattering. The third type of vibrational excitation mechanism involves the creation of a temporary negative ion and is referred to as *resonant electron scattering*.

The HREEL spectra presented in this work were recorded at a sample temperature of 90 K and in both specular ($\theta_i = \theta_r = 60°$) and off-specular ($\theta_i = 60°; \theta_r = 50.8°$) scattering geometry. The energy of the primary electrons was set to 3.7 eV with an overall resolution of ≤ 4 meV, measured as the full width at half maximum (FWHM) of the elastic peak. In the specular spectra of HREELS, the signals contain both dipole- and impact scattering components (see above) [85]. To separate the dipole-scattering components, off-specular spectra consisting of impact-scattering components were measured at a detection angle of 50.8° (corresponding to 9.2° off-specular). The

angular-dependent measurements are useful to characterize the geometrical structure and predominantly the orientation of adsorbates.

Photoisomerization experiments: A viewport at the spectrometer level allows to illuminate the sample at the same position where also the HREEL spectra are recorded (see Fig. 5). For the illumination of the adsorbate-covered surface a pulsed (10 Hz, pulse length: 5 ns) Nd:YAG laser (Quanta-Ray GCR-150, Spectra Physics) at a wavelength of 355 nm (3.5 eV) or laser diodes at wavelength of 405 and 445 nm, respectively, were used. The output power of the individual laser beams was set to $\approx$ 140 mW/cm^2. The laser spatial profiles were characterized by a CCD camera located at a position outside the UHV chamber, which is equivalent to the sample position. Rather large spotsizes with a diameter of $\approx$ 5 mm were chosen to guarantee an overlap between the illuminated area and the electron beam in the HREEL spectrometer.

2.3. Sum-frequency generation vibrational spectroscopy

For SFG spectroscopy, a broadband IR pulse ($\approx$150 fs, 20–30 μJ) with a bandwidth of $\approx$ 200 cm^{-1} (FWHM) is used together with a narrowband visible (VIS) up-conversion pulse of 7.5 μJ at ω_{VIS}= 800 nm. Both beams are p-polarized and focused onto the sample under grazing incidence of $\approx$ 75°. The resulting SFG signal is spectrally dispersed and detected by an intensified CCD camera. Thus, vibrational spectra within a bandwidth of $\approx$ 200 cm^{-1} can be obtained without scanning the IR frequency. Resonant enhancement in the SFG signal will only occur for frequencies ω_{IR} within the bandwidth which are resonant with a vibrational transition (see Fig. 7). Further experimental details are given in Ref. [104].

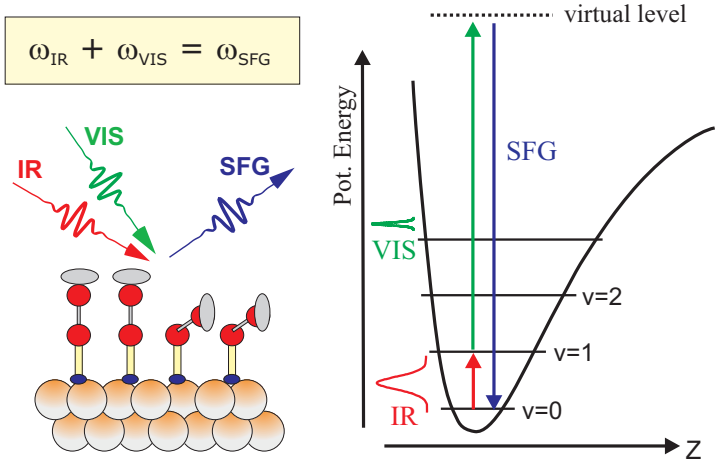

Figure 7. Schematic representation of sum-frequency generation (SFG) vibrational spectroscopy, in which a broadband IR pulse and a narrowband VIS pulse are used to generate SFG. An enhancement of the SFG intensity is observed when the infrared radiation is resonant with a vibrational transition.

SFG is a second-order nonlinear process, which is (in the dipole approximation) forbidden in media with inversion symmetry, and therefore intrinsically sensitive to

interfaces of centrosymmetric media. The SFG intensity is proportional to the second-order nonlinear polarization $\mathbf{P}^{(2)}$ ($\omega_{SFG} = \omega_{IR} + \omega_{VIS}$) induced by frequency mixing in the interfacial region: $I_{SFG} \propto \mid P^{(2)}(\omega_{SFG}) \mid^2 \propto \mid \chi_S^{(2)}(\omega_{IR}) \mid^2 I_{IR} I_{VIS}$, where $\chi_S^{(2)}$ is the interface nonlinear susceptibility (proportional to the number density of interfacial molecules), I_{IR} and I_{VIS} are the intensities of the laser beams at frequencies ω_{IR} and ω_{VIS}, respectively. To lowest order, $\chi_S^{(2)}$ can be described as the sum of a nonresonant term $\chi_{NR}^{(2)}$ and a resonant term $\chi_R^{(2)}$ associated with the vibrational transition ($\chi_S^{(2)} = \chi_{NR}^{(2)} + \chi_R^{(2)}$) describing the probed vibrations as Lorentzians [89]

$$\chi_S^{(2)} = \chi_{NR}^{(2)} + \sum_q \frac{A_q e^{i\phi_q}}{\omega_{IR} - \omega_q + i\Gamma_q} \tag{2}$$

where A_q, ϕ_q, ω_q, and Γ_q are the amplitude of the vibrational resonance, the relative phase, the resonance frequency and linewidth of the qth mode. The nonresonant part $\chi_{NR}^{(2)}$ originates from the nonlinear response of the metal electrons near the surface. The SFG spectra were analyzed using equation 2.

Photoisomerization experiments: For the SFG and photoinduced isomerization experiments the adsorbate-covered substrates were mounted in a chamber and kept under Ar-atmosphere in order to avoid oxidation of the sulfur. For the illumination of the SAM two laser diodes at wavelength of 405 and 470 nm, respectively, were used. The output power of the laser beams were set to 1 mW/cm^2 for the 405 nm and 38 mW/cm^2 for the 470 nm. After a illumination time of $\approx$ 700 s the photostationary state (PSS) was reached. Changes in intensity upon light exposure were simultaneously monitored by SFG.

2.4. Sample preparation

(I) Physisorbed systems: The Au(111) and Ag(111) single crystals were cleaned by a standard procedure of Ar^+ sputtering and annealing. The molecules are dosed by means of a home-built effusion cell held around 380 K at a crystal temperature of 100 K. The adsorbate coverage was quantified by thermal desorption spectroscopy (TDS) and in some cases by work function measurements. Figure 8 shows exemplary thermal desorption spectra of tetra-*tert*-butyl-azobenzene (TBA) adsorbed on Au(111) at different coverages. In the TDS three desorption feature (α_1–α_3) peaking around 314 K (α_1), 400 K (α_2), and 525 K (α_3) are observed which were assigned to the desorption from the multilayer (α_1) and the first monolayer (ML) ($\alpha_2 + \alpha_3$), respectively [61]. Thereby, the monolayer regime contains two desorption peaks (α_2, α_3), where α_2 represents the desorption of $\approx$ 10% of the monolayer coverage (for details see Ref. [61]). In the case of TBA all measurements are performed at a coverage of $\approx$ 0.9 ML, which is prepared by heating the multilayer-covered surface to 420 K. An analogue preparation have been done for the other studied molecules.

(II) Self-assembled monolayer: The gold substrates (200 nm gold evaporated on

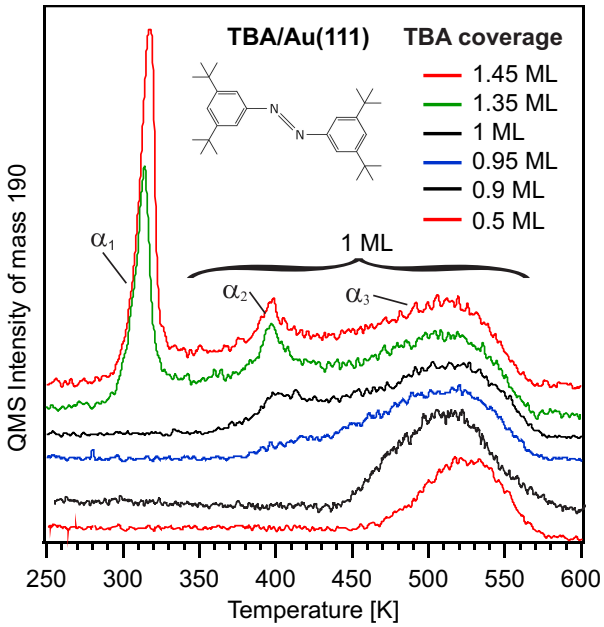

Figure 8. Thermal desorption spectra of TBA on Au(111) at different coverages recorded with a heating rate of 1K/s at the fragment mass of 190 amu (reproduced from Ref. [61]).

quartz) were flame annealed before immersed into a solution of 1 mg of the azobenzene-tripod conjugate (see Fig. 33) dissolved in 2.2 ml of a 2:1 ethanol/THF solution. 15 μl of a 28% aqueous solution of NH_3 was added for the *in-situ* deprotection of the thioacetate and the reaction mixture was degassed for 20 min under a stream of argon. The films were formed by immersion of the gold substrates for 24 h in the dark and under Ar-atmosphere. After immersion the samples were carefully rinsed with copious amounts of THF, dried in a stream of argon and kept in containers filled with argon in the dark until the SFG measurements.

3. Trans/cis-isomerization of molecular switches adsorbed on Au(111)

This chapter describes the studies on the molecular switches azobenzene, stilbene and imine derivatives adsorbed on Au(111), which undergo in the case of the free molecules in solution a *trans/cis*-isomerization. All molecules are specifically designed, i.e., they are equipped with four lateral *tert*-butyl groups (see Figure 9), which are believe to act as "spacer legs" (see chapter 3.3) to reduce the electronic coupling between the optically active molecular orbitals and the metallic substrate.

Varying the functional unit from the diazo- (–N=N–) over the imine- (–N=CH–) to the ethylene- (–HC=CH–) group provides the opportunity to gain a comparative insight into the adsorption, electronic and in particular the switching properties. By means of 2PPE and HREELS we will demonstrate that tetra-*tert*-butyl-azobenzene (TBA) in direct contact with the Au(111) surface undergoes a reversible photoinduced and thermally activated *trans/cis*-isomerization [61, 105, 106, 107, 62]. In contrast, for the

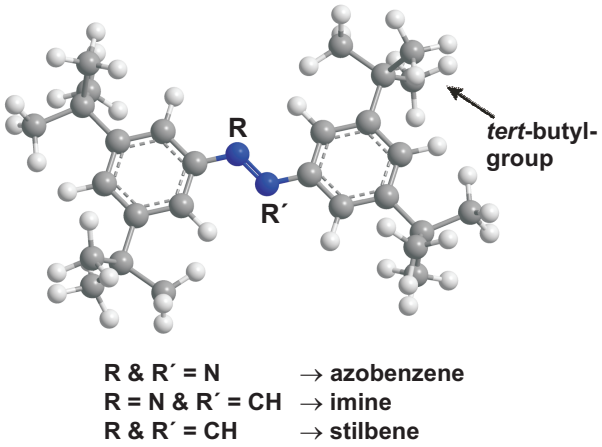

Figure 9. Structure of the molecular switches considered in this study. In addition the 4,4'-dimethoxy-tetra-*tert*-butyl-azobenzene (diM-TBA) has been investigated.

tetra-*tert*-butyl-imine (TBI) [108], tetra-*tert*-butyl-stilbene (TBS) [109] and di-methoxy-tetra-*tert*-butyl-azobenzene (diM-TBA) adsorbed on Au(111) [110], respectively, as well as TBA on Ag(111) [111] no photoinduced conformational changes in the monolayer regime are observed. Presumably this arises from the stronger interaction with the metal substrate and corresponding differences in the geometric and electronic structure as well as the ultrashort lifetime of the excited states. In the case of TBA adsorbed on Au(111), 2PPE and HREELS spectroscopy enabled us to follow the isomerization *via* significant changes in the electronic and geometrical structure, allowing to gain mechanistic and quantitative insight into the switching process. For TBI on Au(111) a reverse situation is found compared to the free molecules in solution, *viz.* at the Au surface the *cis*-isomers possess the thermally stable configuration. Below we present and discuss the results starting with the TBA/Au(111) and diM-TBA/Au(111) followed by TBI/Au(111) and TBS/Au(111). In addition, the role of the bulky tert-butyl groups for the photoisomerization ability will be discussed.

3.1. Reversible molecular switching of tetra-tert-butyl-azobenzene on Au(111)

In the liquid phase azobenzene and its derivatives undergo a photoinduced reversible *trans/cis*-isomerization between the nearly planar *trans*-isomer and the three-dimensional *cis*-form. Therefore the *trans*-isomer exhibits a vanishing dipole moment, while the *cis*-isomer has a dipole moment of 3.2 Debye. In the electronic ground state the *trans*-isomer is by 0.6 eV more stable than the *cis*-form. The photoisomerization is driven by an optical excitation at appropriate wavelengths in the UV (*trans* $\rightarrow$ *cis*) and visible (*cis* $\rightarrow$ *trans*) region followed by either N=N bond rotation or N inversion. In addition, the thermally activated *cis* $\rightarrow$ *trans* reaction is possible which involves an activation energy of around 1 eV [21, 22, 23].

Besides structural studies of azobenzene and its derivatives adsorbed on noble metal surfaces using scanning tunneling microscopy (STM) [112, 113, 114, 115, 116, 117], it has

been shown that azobenzenes can be manipulated with the STM-tip. The manipulations that were achieved are rotations of a phenyl ring and translation of the molecules [118, 119] as well as *trans/cis*-isomerization [64, 65, 67, 120, 121, 122]. Thereby reversible conformational changes have been achieved by resonant [64] and inelastic [65] tunneling and *via* the applied electric field [67]. Photoinduced switching has been demonstrated so far only for a TBA adsorbed on Au(111) [61, 45, 62, 123, 105]. Thereby both the *trans* $\rightarrow$ *cis* isomerization and the back reaction due to UV or visible light exposure at the same wavelength (375 nm or 444 nm) have been observed using low-temperature STM [45, 123]. In addition, we have shown that TBA on Au(111) can be switched bidirectionally by UV-light and thermal activation resulting in reversible changes in the electronic and geometrical structure of TBA on Au(111), as it will be discussed below [61, 62, 105].

3.1.1. Adsorption behavior One of the basic prerequisite for studying molecular switching processes at surfaces is the existence of well-defined adsorbate/substrate-systems in which the molecules possess a defined geometry. To apply spatial averaging techniques like photoemission spectroscopy ordered adsorbate monolayers are chosen.

Low-temperature STM experiments have shown that adsorption of TBA on a Au(111) surface in the sub-monolayer regime leads to the formation of highly ordered islands [67, 45, 68, 116]. Figure 10(a) displays STM images of TBA/Au(111) recorded at a substrate temperature of ≈ 5 K. The molecules are deposited by evaporation from a Knudsen cell with the substrate kept at room temperature. All molecules have the same appearance, i.e., four protrusions with a rhombic shape, which correspond to the four *tert*-butyl groups while the central azobenzene backbone is not visible. The molecules form parallel rows running $\pm(5 \pm 3)^\circ$ with respect to the closed-packed direction of Au(111) [116, 67]. The long axis of the molecules is orientated along one of the closed-packed directions of the substrate and neighboring molecules are aligned with each other. From comparison between the experimental data and simulations of the STM images it has been concluded that all TBA molecules adsorb in the planar configuration corresponding to the *trans*-isomer [116, 67].

To verify if the proposed adsorption geometry is also valid for a coverage of 0.9 ML used in the subsequent experiments (see Section 2.4 Fig. 8) we performed angular-dependent HREELS measurement for TBA adsorbed on Au(111). Figure 10(b) shows HREEL spectra recorded in specular and 9.2° off-specular geometries. In the specular spectrum several vibrational features are observed which have been assigned in Ref. [62]. Here we focus on the intense torsion modes (out-of-plane) of the phenyl rings (τ(C–C)) located at 696 and 879 cm^{-1}. These vibrations show a huge intensity decrease in the off-specular spectrum indicating that their intensity originates mostly from dipole scattering in the specular spectrum. The strong dipole activity of the phenyl ring torsion modes points towards a preferential orientation of the TBA parallel to the Au(111) surface, *viz.* a planar (*trans*)-geometry, since in this orientation these modes have a strong dipole moment change upon vibration perpendicular to the surface. We conclude

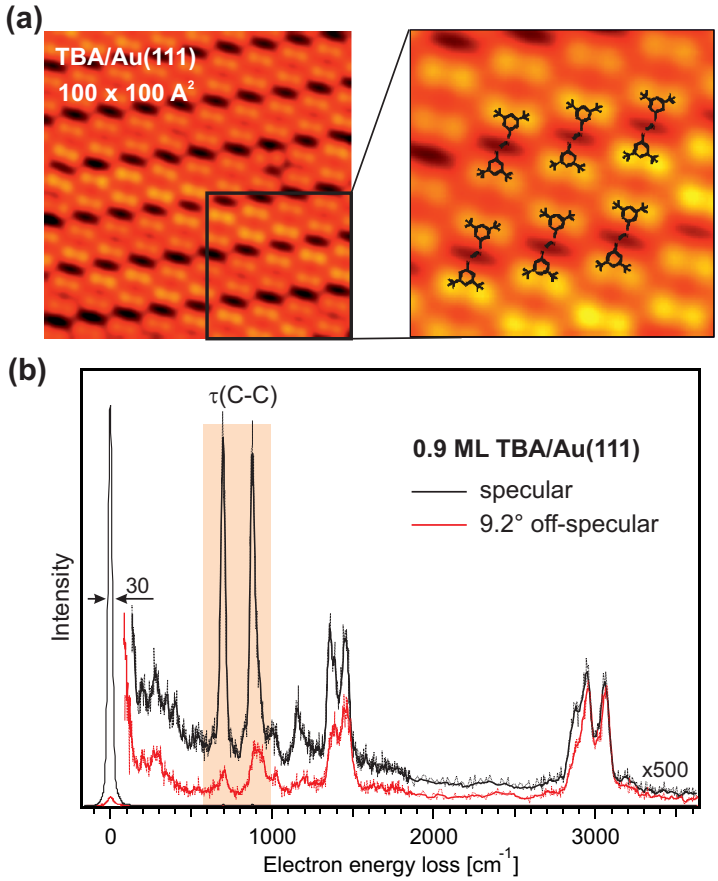

Figure 10. (a) STM images of a TBA island adsorbed on Au(111), courtesy of Leonhard Grill, Fritz-Haber-Institut, Berlin. (b) HREEL spectra of 0.9 ML TBA adsorbed on Au(111) recorded in specular and 9.2° off-specular geometries, with a primary electron energy of 3.7 eV.

that at a coverage of 0.9 ML the TBA adsorbs in the planar (*trans*)-configuration, which is also the energetically most favorable geometry for the free molecule. This adsorption geometry has also be confirmed by near edge X-ray absorption fine structure spectroscopy (NEXAFS) [124] and large-scale density-functional theory (DFT) [125]. For the TBA adsorbed on Au(111) the basic requirement to achieve a well-defined adsorbate system, which is essential in order to study switching processes at surfaces is fulfilled as indicated by STM, HREELS and NEXAFS studies.

3.1.2. Reversible isomerization In the following we investigated the photoinduced and thermally activated *trans/cis*-isomerization of 0.9 ML TBA adsorbed on Au(111). Figure 11 shows schematically the potential energy landscape for the reversible switching process. On the basis of reversible changes in the electronic and vibrational structure observed by 2PPE and HREELS, respectively, it has been shown that both the photo-stimulated *trans* $\rightarrow$ *cis* isomerization as well as the thermally activated back-reaction are operative [61, 62]. On the other hand, a recent STM study observed both the photoinduced *trans* $\rightarrow$ *cis* and *cis* $\rightarrow$ *trans* isomerization during exposure with UV-

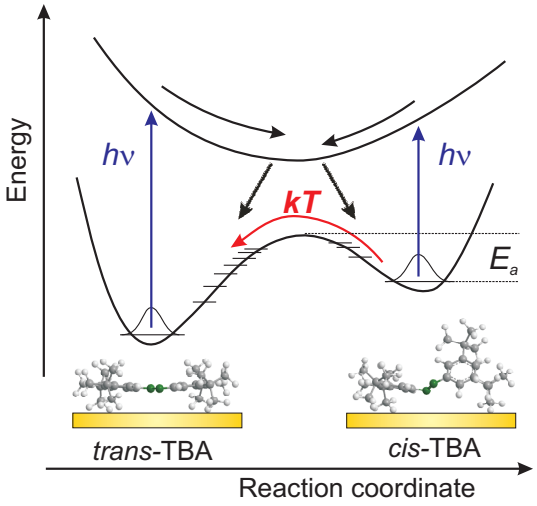

Figure 11. Scheme of the reversible *trans/cis*-isomerization of TBA adsorbed on Au(111) induced by light and thermal activation (for simplicity, only one excited state is shown).

light at 375 nm (3.3 eV), i.e., also the photoinduced *cis* → *trans* reaction is possible [45]. These processes lead to the formation of a photostationary state (PSS) consisting of a mixture of the *trans*- and *cis*-TBA.

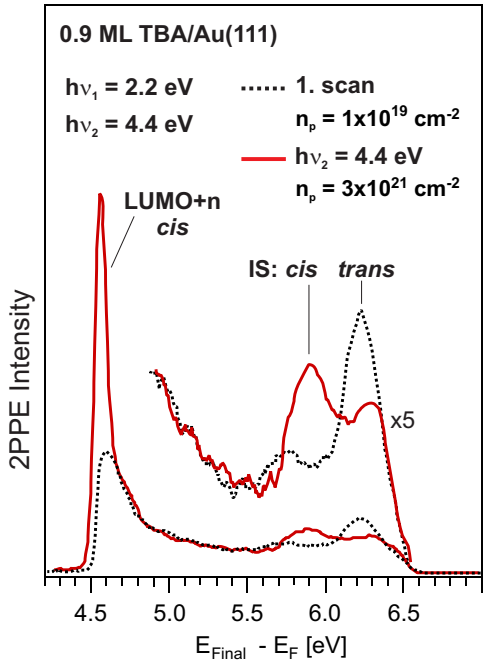

Figure 12. Two-color 2PPE of 0.9 ML TBA adsorbed on Au(111), 1. scan spectrum (recorded for 5 s corresponding to a photon dose of $n_p = 1 \cdot 10^{19} cm^{-2}$) and after illumination at a photon energy of 4.4 eV with a photon dose of $n_p = 3 \cdot 10^{21} cm^{-2}$ measured with 2.2 and 4.4 eV photons. The spectra are displayed as 2PPE intensity versus final state energy with respect to the Fermi level (E_F), $E_{Final} - E_F = E_{kin} + \Phi$ (with Φ the work function), reproduced from Ref. [105]. Note that IS stands for interface state.

Figure 12 represents two-color 2PPE spectra obtained with photon energies of 2.2 and 4.4 eV, which provide access to unoccupied molecular electronic states. Shown are the 1. scan spectrum corresponding to a photon dose (number of photons, n_p) of $1 \cdot 10^{19} cm^{-2}$ and the spectrum after light exposure at 4.4 eV with a photon dose of $n_p = 3 \cdot 10^{21} cm^{-2}$. From the 1. scan spectrum of the adsorbate-covered surface an intense feature from an unoccupied electronic states is observed at $E_{Final} - E_F = 6.25$ eV. This state can be assigned to a delocalized electron resonance with a probability density of the wave function concentrated near the molecule-metal interface (interface state, IS) ‡. It is located at 4.05 eV with respect to E_F for the adsorbed TBA in its *trans*-configuration. Illumination with 4.4 eV photons ($n_p = 3 \cdot 10^{21} cm^{-2}$) leads to an intensity loss of this peak, whereas at slightly lower energy a new feature emerges. We assign this peak to an interface state at the switched TBA (*cis*-isomer)/Au(111) interface. Its energetic position is 3.8 eV with respect to E_F. In addition, close to the vacuum level (which corresponds to the low-energy cut-off of the photoemission spectrum) a strong peak appears due to irradiation, this feature is attributed to an unoccupied final state, LUMO+n of the *cis*-TBA. Note that the assignment of the electronic states has been verified by photon energy [106] and coverage dependent as well as dispersion and lifetime measurements [130].

In comparison scanning tunneling spectroscopy (STS) measurements on individual *trans*- and *cis*-TBA molecules within the ordered island are shown in Figure 13 together with the STM image of the *trans*- and *cis*-TBA [67]. Thereby the isomerization was

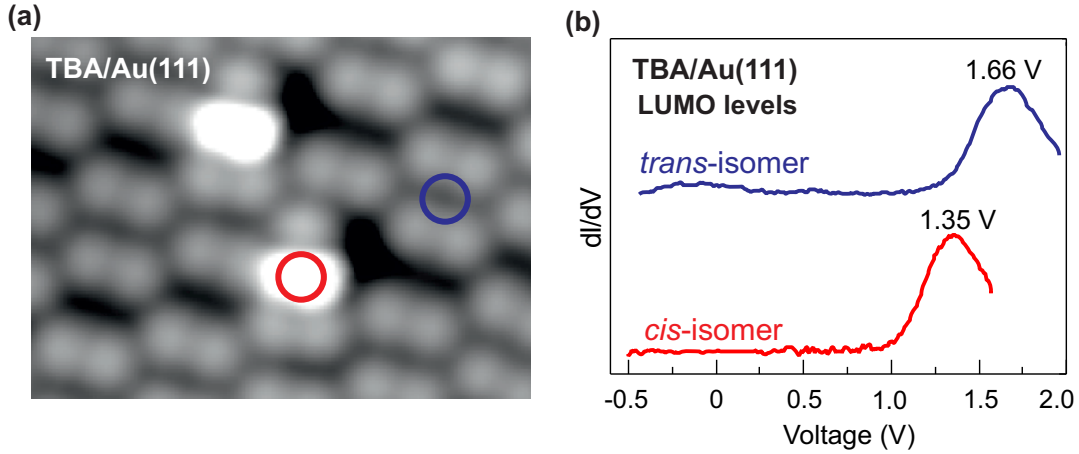

Figure 13. (a) STM image of two *cis*-TBA molecules surrounded by TBA in the *trans*-configuration. The circles mark the positions where the scanning tunneling spectroscopy measurements were performed. (b) dI/dV spectra of the *trans*- and *cis*-isomer. A shift of the LUMO peak of ≈ 300 meV is observed between both isomers; courtesy of Leonhard Grill, Fritz-Haber-Institut, Berlin.

induced by the applied electric field in the STM junction. The *cis*-isomer in the STM

‡ Interface states are explained by the superposition of the molecular or atomic potentials of the adsorbate and the potential created by the image charge at the metal-adsorbate interface [126, 127, 128, 78, 129, 101].

image appears with one bright intensity maximum in the center of the three lateral lobes (see Fig.13 (a)) [116, 67]. Note that in the photo-stimulated isomerization studied by STM, the *cis*-TBA showed exactly the same shape suggesting that the same *cis*-isomer is formed (see below). From STS the LUMO position of the *trans*-isomer has been determined, it is located at 1.67 eV with respect to E_F. For the *cis*-isomer the LUMO is observed at 1.35 eV. Thus the switching process obviously provokes a shift of the LUMO towards lower energy by 300 meV.

The observation of different energetic positions of the interface states for the *trans*- and *cis*-isomer as well as the appearance of the unoccupied final state (LUMO+n) of the *cis*-TBA in the 2PPE can be used as a fingerprint for the reversible switching process. In addition, it allows to make a quantitative analysis of the amount of switched molecules, which will be discussed in the subsequent section (see Sec. 3.1.3).

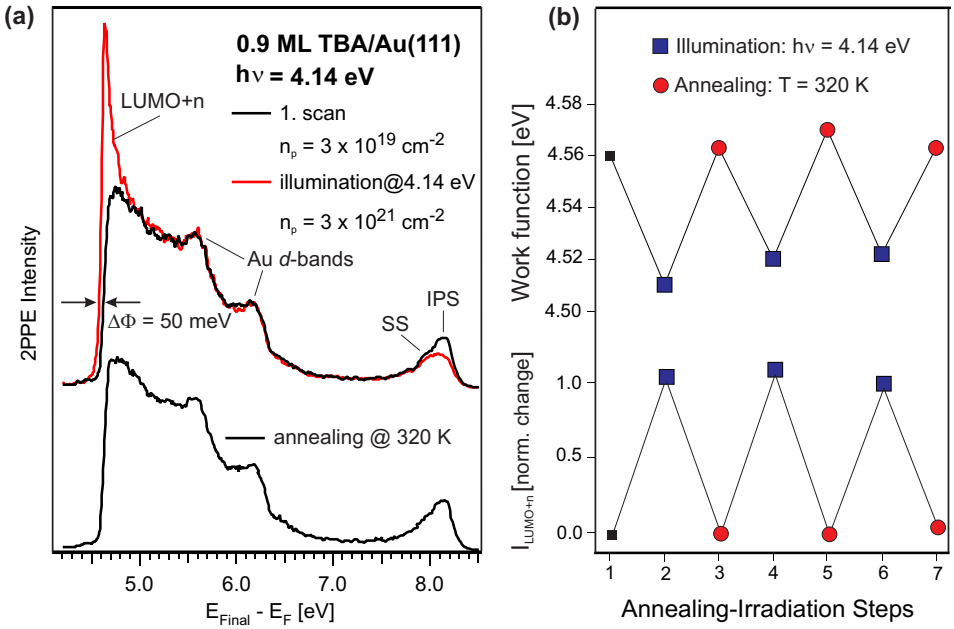

Figure 14. Reversible isomerization of TBA molecules: (a) One-color 2PPE spectra of 0.9 ML TBA adsorbed on Au(111) taken at a photon energy of 4.14 eV. Shown are the 1 scan spectrum ($n_p = 3 \cdot 10^{19} cm^{-2}$), the spectrum after light exposure (4.14 eV) with a photon dose of $3 \cdot 10^{21} cm^{-2}$, and after annealing to 320 K for 300 s. (b) Dependency of the 2PPE intensity of the LUMO+n state and the work function, respectively, on UV-light exposure and annealing.

Figure 14 (a) shows one-color 2PPE spectra, the 1. scan spectrum ($n_p = 3 \cdot 10^{19} cm^{-2}$), after UV-light exposure at 4.14 eV ($n_p = 3 \cdot 10^{21} cm^{-2}$), and after annealing to 320 K for 5 minutes, recorded at a photon energy of 4.14 eV. In the 1. scan spectrum four spectral features are observed: photoemission from the Au *d*-bands [131, 132], which are located at -2.0 and -2.85 eV below E_F, the occupied Shockley surface state (SS) at -0.48 eV [133], and the $n = 1$ image potential state (IPS) at 0.6 eV below E_{vac} [134, 135]. Illumination at 4.14 eV of the TBA-covered surface induced the *trans* $\rightarrow$ *cis* isomerization which is associated with an intensity decrease of the

image potential state, a shift in work function by ≈ 50 meV towards lower energies, and the appearance of the unoccupied final state (LUMO+n) of the *cis*-TBA. The latter two effects are also observed in the two-color 2PPE experiment (see Fig. 12). It is known that 2PPE spectroscopy of image potential states is a very sensitive probe of the adsorbate morphology [136, 137, 138, 139]. In the case of disordered adsorbate layers image potential state peaks are often suppressed or broadened, whereas from ordered layers these peaks are clearly visible. As the adsorbate layer consisting of *trans*-TBA is well-ordered (see section 3.1.1) the loss in intensity of the image state peak after illumination originates from a conformational change of the TBA molecules, *viz.* a change in the morphology of the adsorbate. The shift in the work function is due to the different dipole moments of both isomers. While the planar *trans*-molecule has a vanishing dipole moment the non-planar *cis*-isomer (free molecule) possesses a large dipole moment of 3.6 D [140].

Since it is known that the reverse process, i.e., the *cis* → *trans* isomerization of azobenzene and its derivatives in the liquid phase can also be induced by thermal activation, annealing experiments were performed. In fact, these measurements indicate that by annealing the sample to 320 K the original 2PPE spectrum as recorded in the 1. scan with respect to intensity and shape can be recovered as can be seen in Fig. 14(a). Repetition of the illumination and annealing steps clearly demonstrates the reversibility of the switching process as shown in Fig. 14(b) on the basis of the intensity change of the LUMO+n state and the work function change, respectively.

The reversible isomerization of TBA on Au(111) can also be observed in the vibrational structure of TBA/Au(111) using HREELS as shown in Figure 15. UV-light

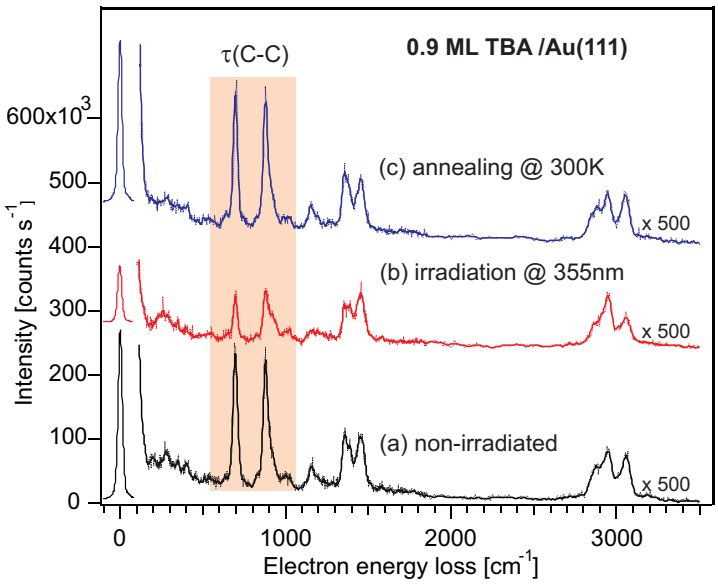

Figure 15. Reversible isomerization of TBA molecules: HREEL spectra of 0.9 ML TBA adsorbed on Au(111) (a) before and (b) after UV-light exposure at 355 nm ($n_p = 2 \cdot 10^{21} cm^{-2}$) as well as (c) after annealing the illuminated sample to 300 K for 300 s recorded with a primary electron energy of 3.7 eV.

exposure at 355 nm (3.5 eV) leads to a significant intensity decrease of the elastic peak and all dipole active modes, most demonstrative for the phenyl ring torsion vibrations (τ(C-C)) at 696 and 878 cm^{-1} due to the *trans*/*cis*-isomerization. One would expect the appearance of new vibrational features, which are associated with TBA molecules in the *cis*-configuration. However, vibrational (IR [141] and Raman [142]) spectra of the *trans*- and *cis*-azobenzene in the condensed phase exhibit only small differences in the vibrational structure between the two isomers. The main difference is a shift of the N=N stretching mode to higher energies from 1443 to 1511 cm^{-1} when going from the *trans*- to the *cis*-form. However, the intense CH_3 bending modes of the *tert*-butyl-groups in the TBA adsorbed on Au(111) are also located in this frequency range, which inhibits the discrimination between the *trans*- and *cis*-isomer *via* the detection of the N=N stretch mode. A possibility to overcome this difficulty would be to deuterate the *tert*-butyl-groups, which would shift the corresponding vibrational modes towards lower energies. Moreover the use of specific marker groups, e.g. cyano (–C≡N) groups, in *meta*- and/or *para*-position of both phenyl rings could support a better identification of an isomerization reaction. On the other hand, substituents like a cyano-group will change the electronic structure of the molecule and it is unclear if this derivative maintains the switching ability (see section 3.2).

Based on the observed STM images and model calculations for the light- and electric field induced *trans* to *cis* isomerization of TBA on Au(111), a molecular structure for the *cis*-isomer has been proposed [67, 45, 116]. In the *cis*-isomer one phenyl-moiety remains parallel to the surface whereas the second phenyl ring is pointing upwards. This geometry has been confirmed by NEXAFS [124] and DFT [125] (see Fig. 11). If we assume the same molecular configuration in our experiment then the strong intensity decrease of the dipole active modes, in particular the phenyl torsion vibrations, can be expected, because in the switched state one phenyl-ring per molecule is no longer orientated parallel to the surface. In addition, the tilted geometry of one phenyl ring in the *cis*-TBA leads to a less-ordered molecular film, resulting in a reduced intensity of the scattered elastic electron beam (diffuse scattering), which causes an intensity drop of all dipole active modes. As observed in the 2PPE experiment, annealing of the TBA-covered surface (see trace (b) in Fig. 15) to 300 K (for 300 s) induces the back-reaction (*cis* → *trans* isomerization), i.e., the same HREEL spectrum with respect to intensity and shape can be retrieved as without illumination (see Fig. 15).

Summarizing, a reversible switching process of surface-bound TBA, which is induced by light and thermal activation could be demonstrated using different experimental techniques, namely 2PPE, HREELS and NEXAFS.

3.1.3. Quantification of the photoinduced isomerization In order to quantify the light-induced isomerization of TBA/Au(111) we evaluated cross sections for the reaction *via* the intensity of the LUMO+n state and the different positions of the interface states of the *trans*- and *cis*-TBA. Since it is known from STM studies that 3.3 eV photons induce both the *trans* → *cis* conformational change and the back reaction

[45] it is likely to assume that also at a photon energy of 2.99 eV used in the present study a photoinduced *cis* → *trans* isomerization is operative. Hence, for the *reversible* photoinduced isomerization, a cross section for both the *trans* → *cis* (σ_{cis}) and for *cis* → *trans* (σ_{trans}) reaction has to be considered.

Since the amount of *cis*-TBA isomers as a function of photon dose is unknown we used the photoemission yield from the unoccupied final state (LUMO+n) of *cis*-TBA as a measure for the switching process, *viz.* we correlated the change in intensity of the LUMO+n peak as a function of photon dose (see Fig. 16(a)) with the number of switched molecules, i.e., $\Delta I \propto [cis]$. In addition, for the detection of the switching process *via* the change in the 2PPE intensity, a two-photon process is required (second-order process) and therefore the 2PPE intensity is proportional to the squared fluence ($\Delta I_i \propto F_i^2$, with F_i the fluence for each pixel i of a CCD camera, which was used to characterize the laser spatial profile [61]). This results in the exponential saturation function:

$$\Delta I_{total} = \sum F_i^2 \Delta I_\infty \left(1 - e^{-(\sigma_{trans}+\sigma_{cis})\cdot F_i \cdot t}\right) . \quad (3)$$

The solid line in Fig. 16 (a) represents a fit according to eq. 3. From this fit one derives a value of $\approx 6 \cdot 10^{-22} cm^2$ for the sum of the cross sections ($\sigma_{trans} + \sigma_{cis}$).

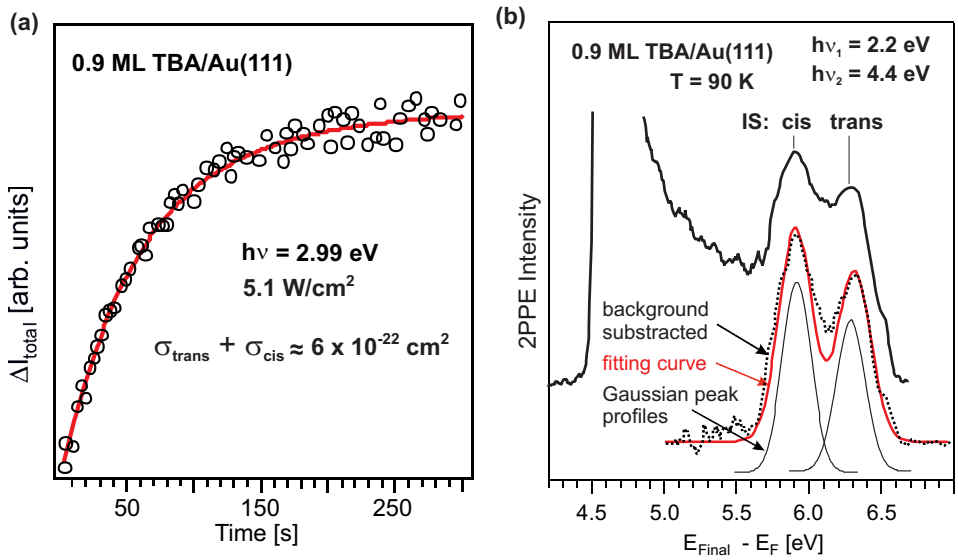

Figure 16. (a) Change in the photoemission intensity of the unoccupied final state (LUMO+n) as a function of illumination time. The solid line represents a fit by using the exponential saturation function eq. 3. (b) Two-color 2PPE of 0.9 ML TBA adsorbed on Au(111) in its photostationary state, showing the interface states of the *cis*- and *trans*-TBA, respectively, adapted from Ref. [105]. The dotted line represents the 2PPE intensity after background substraction, whereas the solid line is a fitting curve using Gaussian peak profiles. From this fit one derives the intensity ratio of the interface states peaks from the *cis*- to *trans*-isomer of ≈ 55/45, and hence the composition of the photostationary state with 55±5% of the TBA molecules in the *cis*-configuration.

In the photostationary state, i.e., in the dynamical equilibrium the temporal change

of the concentration of both isomers is zero, therefore $[cis]_\infty/[trans]_\infty = \sigma_{cis}/\sigma_{trans} = K$ where K is the equilibrium constant. In order to estimate the amount of both isomers in the photostationary state, we exploit the interface state of the *cis*- and *trans*-TBA, which are well separated in the 2PPE spectrum (see Fig. 12). Assuming that the detection of both interface states in 2PPE spectroscopy occurs with the same probability, one can correlate the quantity of each isomer with the peak intensity. Fitting of the peak intensities and shapes using Gaussian peak profiles after background substraction as shown in Figure 16(b) yields a ratio of the interface state peaks from the *cis* and *trans*-isomer of $\approx 55/45$ ($[cis]_\infty/[trans]_\infty = 55/45$). Thus, in the photostationary state $55 \pm 5\%$ of the TBA molecules are in the *cis*-configuration. In comparison, a low-temperature STM study has reported a value of 50% *cis*-TBA in the photostationary state after light exposure at a photon energy of 3.3 eV [123]. The slight discrepancy of $\approx$ 5% between the values might due to the different substrate temperatures of 20 K in the STM experiment compared to 90 K in the 2PPE measurements. In principle, a higher substrate temperature could lead to a different photostationary state, for instance *via* a thermally-assisted photoinduced process.

The cross section for the *trans* $\rightarrow$ *cis* isomerization is by a factor of 1.2 higher compared to the cross section for the back reaction, resulting in an equilibrium constant $K = 1.2$. From the fit according to eq. 3 (see Fig. 16(a)) we obtained for the sum of the cross sections a value of $\approx 6 \cdot 10^{-22} cm^2$, therefore the cross sections for the *trans* $\rightarrow$ *cis* and *cis* $\rightarrow$ *trans* -isomerizations are $\sigma_{cis} = 3.3 \pm 0.5 \cdot 10^{-22} cm^2$ and $\sigma_{trans} = 2.7 \pm 0.5 \cdot 10^{-22} cm^2$, respectively. Note, that the cross section obtained from the photoinduced isomerization at 3.3 eV (375 nm) using low-temperature STM is only $2.3 \cdot 10^{-23} cm^2$ for the *trans* $\rightarrow$ *cis* as well as for the back reaction [123]. This value is approximately one order of magnitude lower than the cross section obtained in the present study. However, temperature dependent measurements indicate that the substrate temperature has a pronounced influence on the photoinduced isomerization efficiency [143].

For comparison the photo-stimulated *trans* $\rightarrow$ *cis* isomerization of TBA in the liquid phase (cyclohexane) yields a *cis*/*trans* ratio of $\approx 89/11$ in the photostationary state after UV-light exposure at 357$\pm$42 nm [116]. Furthermore the *trans* $\rightarrow$ *cis* isomerization cross section for azobenzenes in solution (including TBA) is in the order of $\approx 10^{-19} cm^2$ [22]. Both the smaller amount of *cis*-TBA in the photostationary state and the by three orders of magnitude lower cross section for the surface-bound molecules clearly indicate the strong influence of the interaction with the surface on molecular photoswitching. At a metal substrate effective quenching processes of molecular excitation are operative. In addition steric hinderance effects may play a role, since the molecules lose the freedom to change conformation if the atomic motion is constrained by the surface.

3.1.4. Excitation mechanism in the photoisomerization One of the key questions addresses the excitation mechanism of the photoisomerization of TBA in direct contact with the Au(111) surface. To solve this issue we compare in the following the optical

absorption of TBA in the liquid phase and the light-induced isomerization cross section of surface-bound TBA as a function of photon energy.

For the free azobenzene and its derivatives photoisomerization is induced by direct (intramolecular) optical electronic excitation [21, 22, 23]. Figure 17(a) displays UV-VIS absorption spectra of TBA in solution. The strong absorption band around 3.8 eV belongs to $\pi \rightarrow \pi^*$ (S_2) transition, whereas the band at $\approx$ 2.8 eV corresponds to the symmetry forbidden $n \rightarrow \pi^*$ (S_1) excitation. The intensity loss of the absorption band at 3.8 eV due to illumination at a photon energy of 3.96 eV is assigned to the *trans* $\rightarrow$ *cis* isomerization. Figure 17(b) shows the dependence of the effective cross section

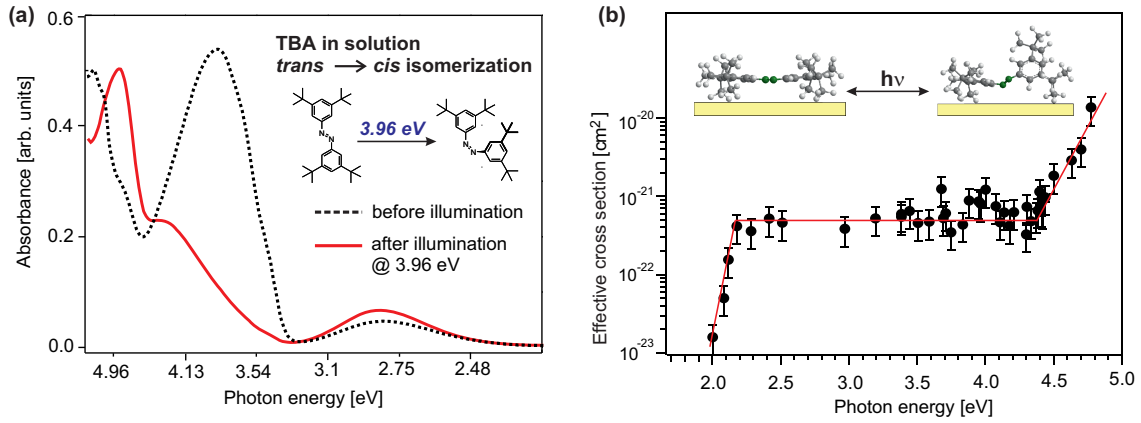

Figure 17. (a) UV-VIS absorption spectra of TBA in cyclohexane before and after illumination with UV-light at 3.96 eV. Exposure at 3.96 eV leads to a decrease of the absorbance around 3.81 eV which is due to the *trans*/*cis*-isomerization. (b) Effective cross section for the photoinduced *trans*/*cis*-isomerization of TBA adsorbed on Au(111) as a function of photon energy (see text); reproduced from Ref. [106].

(σ_{eff}) for the light-induced *trans*/*cis*-isomerization of TBA adsorbed on Au(111) on the photon energy used for excitation. σ_{eff} is determined by evaluating the peak intensity of the unoccupied final state of the *cis*-isomer (LUMO+n) as a function of photon dose for various photon energies using the exponential saturation function, eq. 3 (see Fig. 16 (a)). Thereby the initial slope of the exponential function as well as the saturation level, i.e., the ratio between the photoemission intensity of the LUMO+n state in the photostationary state and the intensity of the 1. scan spectrum is obtained. This ratio is identified with the amount of switched *cis*-TBA in the photostationary state and we have verified that it stays constant over the whole photon energy regime between $\approx$ 2.0 and 4.8 eV.

As seen in Fig. 17 (b), σ_{eff} shows a stepwise change, a plateau like region over the large photon energy range between 2.2 and 4.4 eV, where it stays constant. Above 4.4 eV a strong exponential increase and below 2.2 eV a pronounced decrease are observed (note the logarithmic scale). Below a photon energy of 2 eV isomerization of TBA has not been observed. The shape of σ_{eff} as a function of photon energy, particularly the constant cross section over the large photon energy range between 2.2 and 4.4 eV as well as the threshold like behavior below 2.2 eV and above 4.4 eV, is very unusual for

photochemical reactions of adsorbates on metal surfaces [29, 30]. Note, that also no resonance is observed in contrast to the wavelength dependence in the liquid phase.

In order to determine the excitation mechanism in the photoinduced isomerization one has to consider the electronic structure of TBA/Au(111) as well as the density-of-states of the gold substrate. Table 1 summarizes the binding energies of all electronic states observed by 2PPE [106]. The Fermi level of Au(111) serves as the reference. The vacuum level is identified by the work function of the TBA-covered surface, which is 4.45 eV. In the following, we will discuss the excitation mechanism of the photoinduced

$E - E_F$ [eV]	Assignment
4.8	LUMO+m
4.45	LUMO+n (*cis*-TBA)
4.05	interface state (*trans*-TBA)
3.80	interface state (*cis*-TBA)
1.7	LUMO (*trans*-TBA)
-0.48	$n = 0$ (Shockley surface state)
-1.8	HOMO
-2.0	Au *d*-band
-2.85	Au *d*-band
-3.0	HOMO-1

Table 1. The energies of the photoemission spectral features of 0.9 ML TBA absorbed on Au(111). All features are referenced to the Fermi level of Au(111).

isomerization on the basis of the observed electronic structure of TBA/Au(111) and the photon energy dependency of σ_{eff}. With the HOMO level located at -1.8 eV and the LUMO position at 1.7 eV (*trans*-TBA), a HOMO-LUMO gap of 3.5 eV is obtained. A direct electronic excitation within the adsorbate like in the liquid phase, i.e., a HOMO-LUMO transition, is incompatible with the observed photon energy dependence of the effective cross section (see Fig. 17(b)), since no resonance in the cross section is observed in this energy region. Note that the width of the LUMO peak is only ≈ 250 meV (data not shown here), but the plateau region of σ_{eff} extents over more than 2 eV. Hence we exclude an intramolecular excitation. An alternative scenario is a substrate-mediated photochemical process, where hot electrons (or holes) are attached to the adsorbate, creating a transient negative (or positive) ion. In the photoinduced chemistry on metal substrates such indirect excitation mechanisms, *viz.* the formation of an anionic state by a transient molecular resonance plays a key role in many surface reactions. In particular, desorption or dissociation of adsorbates are the simplest photoinduced reactions which have been shown to be induced by indirect (charge transfer) excitations [29, 30, 31, 32, 33, 34, 144, 145]. Hot hole induced processes are well-known from the photochemistry of adsorbates on semiconductors surfaces [31, 35, 36, 37, 38, 39].

We consider first the generation of a negative ion resonance as a possible excitation mechanism for the isomerization reaction. With the LUMO level located around 1.7 eV above E_F one would not expect a pronounced drop in σ_{eff} at energies below 2.2 eV. Moreover below a photon energy of 2 eV switching of TBA is not observed. In addition, with increasing photon energy the population of hot electrons, which are resonant with

the LUMO level should increase nonlinearly and thus the probability for the formation of a negative ion resonance should be enhanced. However, since σ_{eff} as a function of photon energy is constant over the wide energy region between 2.2 and 4.4 eV and decreases exponentially below 2.2 eV, we conclude that electron transfer from the metal to the LUMO can not be the dominant excitation process responsible for the switching.

Instead, we propose the following mechanism (see Fig. 18(a)): Light exposure with photon energies higher than ≈ 2.2 eV leads to photo-excitation of holes in the Au *d*-band (electron-hole pair formation, step 1) which rapidly relax to the top of the *d*-band *via* Auger-decay (step 2). These hot holes undergo a charge transfer process to the HOMO level of TBA, thus producing a positive ion resonance (step 3) as schematically shown in Figure 18(a). In the photoemission spectrum (data not shown here) the spectral features

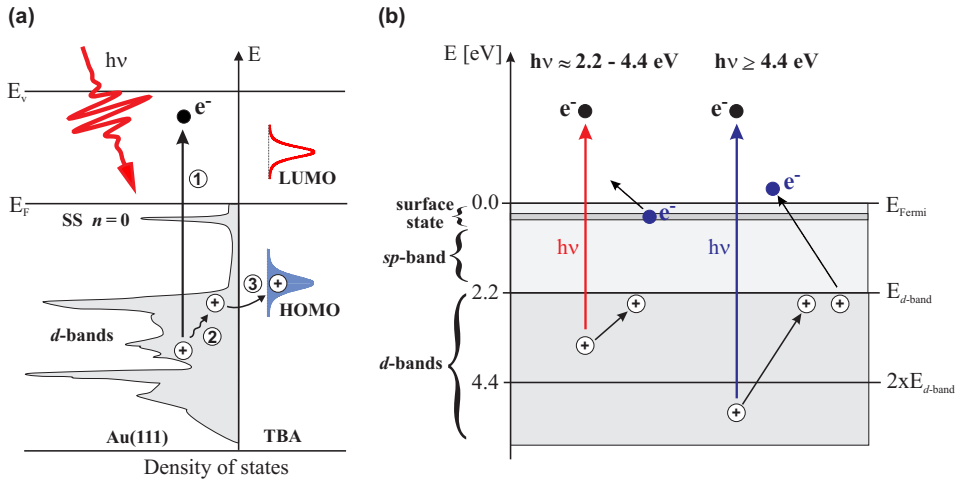

Figure 18. Proposed excitation mechanism for the photoinduced trans/cis isomerization of TBA adsorbed on Au(111) *via* the creation of a positive ion resonance. Thereby photoexcitation at photon energies above ≈ 2.2 eV leads in a first step to electron-hole pair formation. The holes in the Au *d*-band relax to the top of the *d*-band (step 2) followed by a hole transfer to the HOMO of TBA (step 3). (b) Formation of holes in the Au *d*-bands for different photon energies. For photon energies ≥ 4.4 eV, i.e., twice the energy of the *d*-band edge, the population of holes at the top of the *d*-band is enhanced due to Auger-decay processes (see text).

from the Au *d*-band and the HOMO level exhibit some overlap [106]. Therefore it is likely to assume that some degree of hybridization between the HOMO and the Au *d*-band is existent, even though it is expected that the four lateral *tert*-butyl groups should lead to an increased distance of the molecule (see chapter 3.3) and therefore to a reduced electronic coupling between the molecules and the metal surface. Due to the high density of states of the Au *d*-band direct interband transitions to unoccupied states above the Fermi level of gold are efficient for $h\nu > 2.2$ eV, i.e., most of the absorbed photon energy is deposited in *d*-holes rather than hot electrons [97]. It has been shown for copper (with a *d*-band edge comparable to gold) that holes in the *d*-band primarily float up to the top of the *d*-band on a ultrashort timescale of few femtoseconds *via* electron-electron scattering (see Fig. 18(b)). At the top of *d*-band the *d*-hole lifetime is

substantially long, *viz.* in the order of 24 fs for Cu(111) [146, 147, 148, 149]. As a similar electron dynamics can be expected for Au [147, 148, 149] the proposed mechanism of hole relaxation and transfer appears highly plausible. In the case of TBA adsorbed on Ag(111) the HOMO level of TBA is also observed at -1.8 eV with respect to E_F but light-induced switching could not be achieved [111], presumably due to the lower lying *d*-band in silver (Ag *d*-band edge $\approx$ -4 eV). Hence, hybridization between the *d*-band and the HOMO and accordingly a hole transfer should not occur on Ag.

The threshold like behavior of the effective cross section as a function of photon energy, i.e., the decrease below 2.2 eV and the increase above 4.4 eV is related with the *d*-band density-of-states (DOS) and the hole formation process after photoexcitation. The first threshold around 2.2 eV corresponds to the energy of the *d*-band edge, *viz.* the minimum energy required to create a single hole in the Au *d*-band. The second threshold at 4.4 eV matches with twice the energy of the *d*-band edge (see Fig.18(b)). Above this energy ($\geq$ 4.4 eV) photoexcited holes can relax *via* Auger decay resulting in the creation of a second *d*-band hole as schematically shown in Fig 18(b). As a consequence the population of holes at the top of the *d*-band is enhanced compared to hole formation in the energy regime below 4.4 eV and correspondingly this leads to an enhanced switching rate. The exponential increase of σ_{eff} above $h\nu \approx 4.4$ eV as well as the decrease below $h\nu \approx 2.2$ eV is related to the DOS of the Au *d*-band and *sp*-band, respectively. Note, that the onset of the *d*-band starts around 2 eV and the DOS rises with increasing binding energy as schematically shown in Fig. 18(a). These pronounced variation in the DOS govern the hole relaxation process *via* Auger decay.

The threshold effect on the photoisomerization efficiency due to the abrupt change in the DOS between the *sp*- and *d*-band is comparable with substrate-mediated photochemical processes in semiconductors [31]. Thereby a common observation is the correlation of the photon energy threshold with the band-gap of the substrate. Unlike metals, where scattering between excited carriers and conduction electrons near the Fermi level (Auger decay) is the dominant relaxation process, electron-electron scattering is less important in semiconductors due to blocking of Auger decay by the gap. Therefore excited electrons (or holes) mainly relax *via* electron-phonon scattering on a picosecond timescale. As a consequence the lifetime of the thermalized electrons (or holes) at the band edge can be in the order of nanoseconds, hence significant longer compared to the lifetime of holes at the band edge of noble metals like Au or Cu. While on semiconductor surfaces, e.g. in semiconductor photocatalysis, hole induced processes are quite common [35, 36, 37, 38, 39], such processes are rare for metal surfaces. We note, however that a hole driven photochemical reaction at a metal surface has been proposed in the femtosecond surface chemistry of O_2/Pd(111), but contrary to the present study no direct experimental evidence for such a process was provided [150].

An alternative pathway for photoinduced switching at photon energies above 4.4 eV could be the formation of a negative ion resonance where hot electrons are attached to an unoccupied final state (LUMO+n). Quantum chemical calculation suggested the unoccupied final states to be antibonding orbitals of π-symmetry located at the phenyl

rings [111]. However, for the free molecule in solution these orbitals are not involved in the isomerization process therefore it is reasonable to assume that this is also valid for the surface-bound TBA.

Our findings show that in the light induced excitation mechanisms for molecular switching at a metallic substrate the metal and not the molecule may act as the "chromophore", i.e., the metal is the light-harvesting material in contrast to the photoinduced isomerization of molecular switches in the liquid phase. This clearly demonstrates that adsorption on a metal surface causes significant modifications to the mechanism known in liquid phase.

3.1.5. Thermally-driven isomerization To gain insights in the kinetics of the thermally activated *cis* → *trans* isomerization we determined the rate constant (k), the frequency factor (k_0) and the activation energy (E_a, thermal barrier). Thereby we analyze the change in the photoemission intensity of the LUMO+n state as a function of temperature: The adsorbed *trans*-TBA was illuminated until the photoemission intensity of the unoccupied final state of the *cis*-isomer (LUMO+n) reached saturation (photostationary state). Subsequent annealing experiments were performed and the loss in intensity of the LUMO+n state as a function of temperature was measured. Using an Arrhenius type expression $I = I_0 \cdot exp(-E_a/k_BT)$, where I is the peak intensity of the LUMO+n state, I_0 is the initial peak intensity, k_B is the Boltzmann constant, and T is the temperature, allows calculation of E_a to be 240 ± 30 meV (see Fig. 19 (a)). The rate constant (k) determined from isothermal measurements for different substrate temperatures (data not shown here) [105], the Arrhenius expression ($k = k_0 \cdot exp(-E_a/k_BT)$), and the activation energy obtained from the measurements presented in Figure 19 (a) were used to achieve a frequency factor of $k_0 = 10^{6\pm1}s^{-1}$ shown in Figure 19 (b). The value of k_0 is considerably smaller than the frequently assumed value of $k_BT/h \approx 10^{12}s^{-1}$ (where h is the Planck constant) expected from transition-state theory. The strongly reduced frequency factor can be related to a lowering of the entropy in the transition state caused by the reduction of molecular degrees of freedom in the adsorbed state, i.e., the reaction is sterically strongly hindered. Note that a similar k_0 value has been reported for a thermally induced rotation of a phenyl endgroup of an organic molecule adsorbed on a Au(111) surface [151].

The corresponding values for the activation energy and the frequency factor obtained for TBA in cyclohexane solution are E_a= 1.0 eV and $k_0 \approx 1.6 \cdot 10^{10}s^{-1}$ [105]. Quantum chemical calculations yield a value of 1.02 eV for the activation energy and a frequency factor in the order of $4 \cdot 10^{13}s^{-1}$ for the free molecule [152]. While the activation energies obtained in both phases are equal, the frequency factor in solution is three orders of magnitude smaller, reflecting the influence of the solvent on the molecular degrees of freedom in the transition state.

A key finding is, that both E_a and k_0 for the surface-bound TBA are strongly reduced compared to the values for the isomerization of TBA in solution (see inset of Fig.19 (a)). The pronounced reduction of E_a for the thermally-induced isomerization

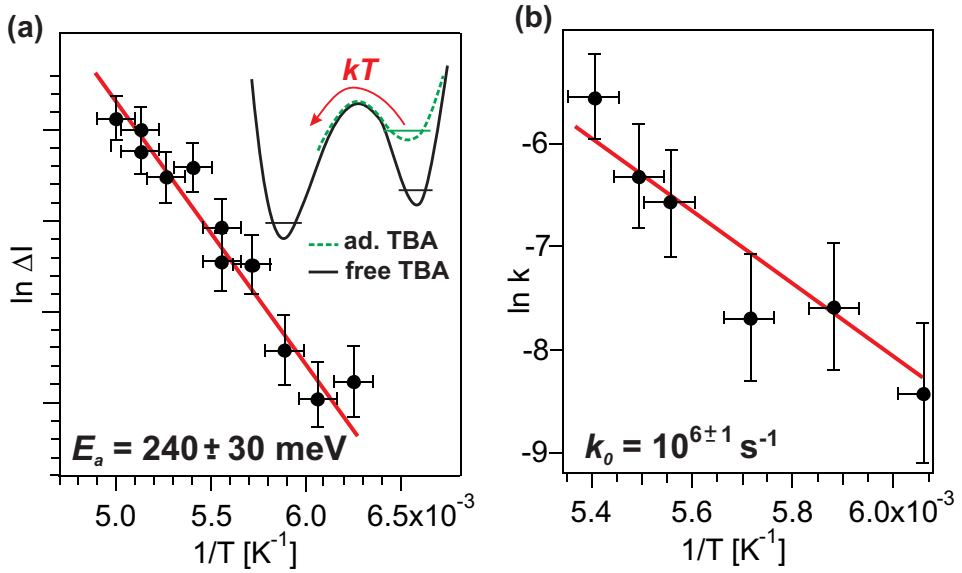

Figure 19. Kinetic analysis for the thermal *cis* → *trans* isomerization of adsorbed TBA. (a) Arrhenius plot to evaluate the activation energy (E_a). Inset: Comparison between the potential energy landscape for the thermally activated *cis* → *trans* isomerization for the free and adsorbed TBA (ad. TBA) molecules, indicating the strong reduction of the thermal barrier for the surface-bound molecules. (b) Determination of the frequency factor (k_0) by means of the Arrhenius expression and the activation energy obtained in (a) (reproduced from Ref. [107]).

of TBA on Au(111) by a factor of four clearly reflects the effect of electronic coupling between the metal surface and the adsorbed TBA, *viz.* the potential energy surface for the isomerization must be very different from that in the liquid phase. This is surprising, since it was expected that the four lateral *tert*-butyl groups should lead to an increased distance of the molecule and therefore to a reduced coupling between the molecule and the metal surface. However, based on the proposed mechanism for the photoinduced isomerization of TBA on Au(111) (see section 3.1.4), it becomes evident that still a sufficiently strong electronic coupling must be existent, presumably *via* the N=N bonding or the lone pairs of the nitrogen.

3.2. Reversible isomerization of a decoupled molecular switch

Motivated by the work on TBA/Au(111) we investigated the adsorption behavior and the switching properties of 4,4‘-di-methoxy-3,3‘,5,5‘-tetra-*tert*-butyl-azobenzene (diM-TBA) adsorbed on Au(111) using HREELS [110]. The motivation of this study is to utilize the methoxy-group as a marker group for the vibrational spectroscopy in order to monitor the switching process as well as to investigate the effect of the changed electronic structure of the molecules due to the methoxy-substituents compared to TBA.

For a coverage of 1 ML as well as for 2 ML the phenyl ring torsion and O–CH_3 stretch modes possess a strong dipole activity indicating that diM-TBA adsorbed in the planar (*trans*)-configuration similar to TBA. In contrast to TBA adsorbed on Au(111)

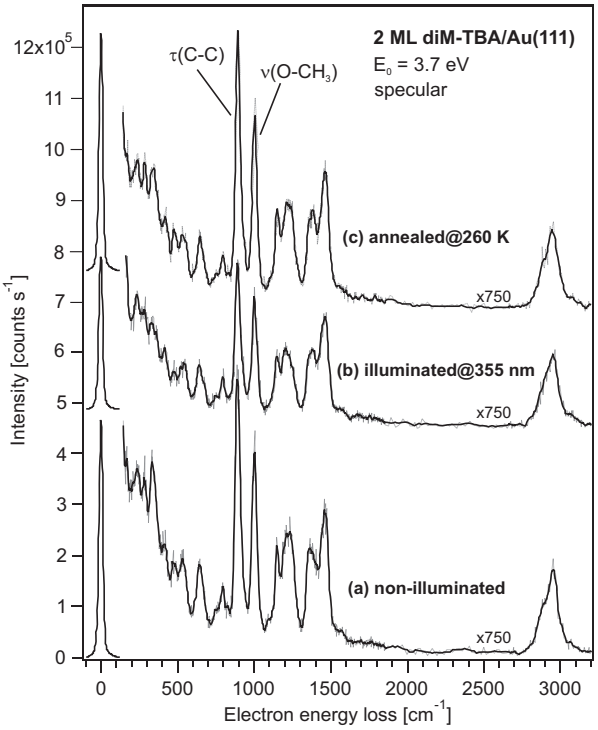

Figure 20. Reversible switching of diM-TBA molecules induced by light and thermal activation. HREEL spectra of 2 ML diM-TBA adsorbed on Au(111) (a) before and (b) after UV-light exposure at 355 nm ($n_p = 1 \cdot 10^{21}$ photons/cm^2) as well as (c) after annealing the illuminated sample to 260 K for 300s recorded with a primary electron energy of 3.7 eV (reproduced from Ref. [110]).

in the monolayer regime, no switching and the corresponding changes in the vibrational structure due to UV-light exposure at 3.5 eV is observed. This fact might be attributed to a different electronic structure and/or adsorption behavior of the molecules compared to TBA/Au(111). The methoxy-groups act as electron donors *via* a resonance mediated $+M$-effect thus they have an influence on the electronic structure, i.e., energetic position of the unoccupied (LUMO) and occupied states (HOMO). In order to elucidate the different performance of diM-TBA a detailed knowledge about the electronic structure of the molecules adsorbed on Au(111) is essential. However, illumination ($h\nu = 3.5$ eV) of the second diM-TBA layer yielded to pronounced modification in the vibrational spectra. As can be seen in Figure 20 light exposure leads to an intensity decrease of the phenyl-ring torsion vibration (at 895 cm^{-1}) and the O–CH_3 stretch mode (at 1009 cm^{-1}). For detailed assignment of all vibrational features see Ref. [110].

After annealing to 260 K these peaks are recovered with respect to shape and intensity. We assign the reversible changes in the vibrational structure to *trans/cis*-isomerization of the diM-TBA molecules. In the second monolayer, which is electronically decoupled from the metallic substrate switching is obviously possible, reflecting the strong influence of the adsorbate-substrate interaction on the molecular switching at metal surfaces. We propose that the photoisomerization is driven by a direct

(intramolecular) electronic excitation of the adsorbed diM-TBA molecules in the second ML analogous to diM-TBA in the liquid phase, since the second layer is decoupled from the metallic substrate and the excitation wavelength used to induce the isomerization (3.5 eV) corresponds to the maximum of the absorption band for the $\pi \longrightarrow \pi^*$ (S_2) transition [110]. Note that for the carboxy-benzylideneaniline adsorbed on Au(111) an identical isomerization behavior has been observed, i.e., a photoinduced and thermally activated reversible trans/cis-isomerization in the second decoupled layer [153].

3.3. Role of the spacer groups

The ability to align molecules on surfaces where they can perform functions such as switching is a major capability in the quest for a molecular nanotechnology. For this purpose, the interaction between their functional units and the substrate must be tailored carefully. This often requires tuning of the coupling to a (metal) surface to protect the molecular functionality against detrimental influences from the substrate, such as quenching of excited states. A wide-spread strategy to control this coupling is the attachment of bulky spacer, e.g. *tert*-butyl-groups which are designed to lift the functional unit of the molecule from the surface [26, 27]. This strategy has also been applied in the case of the azobenzene derivative TBA, which maintains its photoisomerization ability on the Au(111) (see chapter 3.1) in contrast to the parent (unsubstituted) azobenzene [130]. This finding apparently supports the validity of the concept of geometric decoupling using bulky spacer groups as schematically shown in Figure 21 (a) and (b).

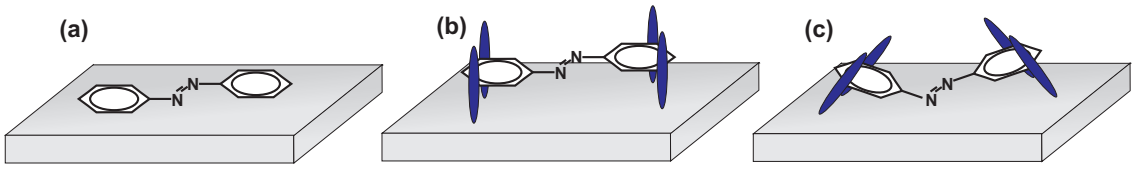

Figure 21. Schematic illustration of the decoupling strategy and its failure in the context of the adsorbed azobenzene switch: (a) parent (unsubstituted) azobenzene, (b) expected lift-off by the bulky spacer (tert-butyl) groups and (c) real adsorption geometry according to NIXSW and DFT (reproduced from Ref. [154]).

However based on precise measurements of molecular adsorption geometries for azobenzene-based switches using the normal incidence X-ray standing wave technique (NIXSW) and corresponding large-scale density-functional theory (DFT) calculations we demonstrate that this widely-used approach is not appropriate and should be replaced by a holistic decoupling strategy which considers the geometric and electronic properties of the entire molecule-substrate complex. If the observed maintenance of the isomerization ability in the TBA on Au(111) is just a consequence of geometric decoupling, achieved through a modified molecular gas-phase structure that remains undistorted on adsorption, one would expect this concept to work irrespective of the substrate material. Instead even on the closely related Ag(111) surface, neither

azobenzene nor TBA could be photoisomerized [111]. To understand the reason behind this failure, we analyzed the detailed adsorption geometry of TBA and azobenzene on Ag(111) with NIXSW [154, 155].

NIXSW allows model-free measurements of vertical adsorption heights above single crystalline surfaces, with an accuracy of about 0.05 Å [156, 157, 158]. It is thus an ideal tool to determine the vertical bonding distances between the photoactive functional diazo (-N=N-) unit in adsorbed azobenzene or TBA, thereby directly addressing the validity of the geometric decoupling concept displayed schematically in Fig. 21 (a) and (b). In the X-ray standing wave field, the photoelectron intensities from the various atoms of an adsorbed molecule depend on their respective distances to the Bragg planes of the substrate. Essentially, this height information can be separately retrieved for each chemical species from the dependence of the corresponding photoelectron yield on the energy of the incident X-ray beam [156, 157, 158].

Analyzing the photoelectron yield for the diazo-group in TBA [154] and azobenzene [155] on Ag(111) (data not shown here), we determine a N-Ag adsorption distance d_{N-Ag} of 3.21±0.05 Å for TBA and d_{N-Ag} = 3.07±0.02 Å for azobenzene. Remarkably, the value for TBA is only 0.14 Å larger than the corresponding value for azobenzene/Ag(111). DFT calculations with a correction scheme to include the dispersive van der Waals interactions [155] quantitatively confirm this trend: For TBA/Ag(111) we calculate d_{N-Ag} = 3.11 Å, only 0.13 Å larger than for azobenzene/Ag(111) (2.98 Å [155]). If the *tert*-butyl groups in TBA indeed served as effective geometrical spacers, i.e. if the idea of a vertical lifting of the central flat "table" moiety as sketched in Figs. 21 (a) and (b) was correct, a much larger distance difference of 1.70 Å would be expected from the respective gas-phase molecular geometries. The reason why this difference is much smaller at Ag(111) is that the real TBA adsorption geometry as determined by our DFT calculations is much better characterized as the "suspended bridge" between tilted *tert*-butyl legs as shown in Fig. 21 (c).

While the experimental and theoretical analysis thus rationalizes why TBA switches as little as azobenzene on Ag(111) - essentially because the spacer group concept fails entirely - it still leaves the puzzle why TBA does switch on Au(111). To further elucidate this we are encouraged by the quantitative agreement between experiment and theory that was reached for the adsorption geometries at Ag(111). Carrying out corresponding calculations for TBA and azobenzene on Au(111), we arrive at the surprising finding that also here there is only an insignificant difference between the adsorption heights: 3.22 Å for azobenzene versus 3.28 Å for TBA. So, also on Au(111) the -N=N- switching unit is not lifted by the spacer groups [154].

These similarities in the adsorption geometries of azobenzene and TBA at Ag(111) and Au(111) largely disprove the purely geometrical arguments that are at the heart of the bulky spacer group concept. Instead, the present analysis supports the suggestion [105] that for both the loss and preservation of the photoisomerization ability the detailed electronic structure of the metal substrate is much more important than previously thought. In particular, the different position of the *d*-band in Ag (≈ -4eV) and Au (≈

-2.1eV) seems to be a key factor in determining the differences observed for these two substrates (see chapter 3.1.4). In our excitation model, we explain the switching/non-switching of TBA on Au(111) and Ag(111), respectively, by assuming that the incident photon creates a hole in the metal, which rapidly relaxes to the upper edge of the *d*-band. In the case of Au(111) this hole can then efficiently transfer to the highest occupied molecular orbital (HOMO) of TBA, in contrast to Ag(111) where the lower lying *d*-band and correspondingly reduced overlap with the HOMO prevent this process. While the details of this model remain to be confirmed, it is clear that the existing data is difficult to reconcile without invoking new substrate-mediated isomerization mechanisms. Working on the assumption of an unchanged isomerization mechanism and simply trying to engineer the distance between molecule and substrate is then a fundamentally flawed approach to tune the switching ability.

In conclusion, the present example of azobenzene-based molecular switches demonstrates that tuning the functionality of adsorbed molecules can only be successful if both the geometric and electronic structure of the complete molecule-substrate complex are taken into account.

3.4. Inverted isomerization behavior: tetra-tert-butyl-imine on Au(111)

Imine is an azomethine that is structurally similar and isoelectronic to azobenzene [159]. In spite of this, the UV-vis spectrum of imine is remarkably different from the spectrum of azobenzene [160]. According to experimental [24, 25] and theoretical [161, 162] studies the main reason for this difference is the non-planar configuration of *trans*-imine, which is caused by the conjugation between the aniline ring (i.e., the phenyl-ring which is connected to the nitrogen) and the nitrogen lone pair. Thereby the torsion angle about the N-phenyl bond is around 55° and the torsion of benzylidene ring (i.e., the phenyl-ring which is connected to the carbon) is around 10° [25] (see Fig. 1). Optical excitation in the UV region ($\approx$ 313 nm) followed by either CH=N bond rotation or N inversion leads to the *cis*-isomer. The activation barrier for the thermal relaxation (*cis* $\rightarrow$ *trans*) is rather low, *viz.* around 0.7 eV and possess a slight dependence on the polarity of the solvent. Thus the ground state relaxation is quite rapid with a rate of $\approx$ 1 s^{-1} at room temperature. Therefore the detection of the *cis*-isomer for instance with vibrational spectroscopy is only possible at temperature below 173 K [163]. So far, investigations on imine and its derivatives adsorbed on (metallic) substrates are rather limited [153, 101, 108].

By employing HREELS we will demonstrate that at a metallic substrate a *cis*-like isomer of tetra-*tert*-butyl-imine (TBI) is the stable configuration contrary to the free molecule in solution.

In order to study the adsorption geometry of TBI on Au(111) angular-dependent HREEL measurements were performed. Figure 22 shows HREEL spectra of 0.5 ML TBI/Au(111) recorded in specular and 9.2° off-specular geometries. The adsorbate-covered surface was prepared at a sample temperature of 210 K. In the specular spectrum

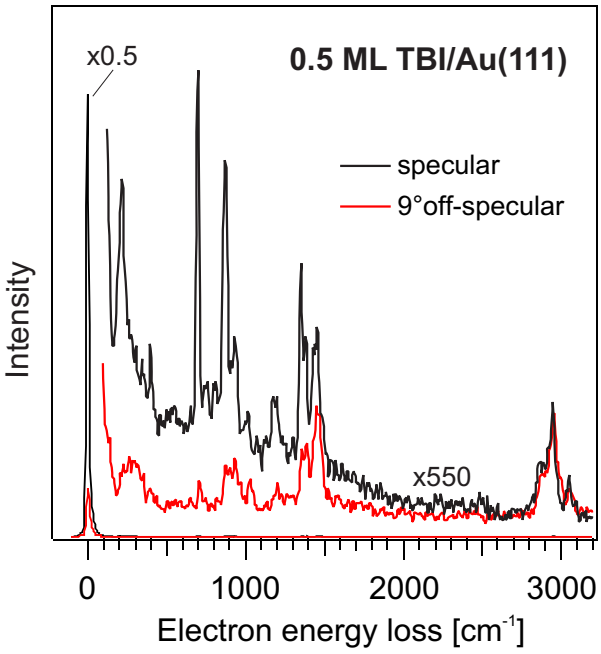

Figure 22. HREEL spectra of 0.5 ML TBI adsorbed on Au(111) recorded in specular and 9.2° off-specular geometries, with a primary electron energy of 3.7 eV (reproduced form Ref. [108].

several vibrational features are detected, here we discuss only the angular dependency of the vibrational modes which are relevant for the determination of the adsorption geometry. Strong vibrations of the phenyl ring torsion (out-of-plane, τ(C–C) at 705 and 877 cm^{-1}) and the C–H deformation (out-of-plane, γ(C–H) at 927 cm^{-1}) are observed. Among the vibrational modes caused by the excitation of the *tert*-butyl-groups weaker feature of the C–C and N–C stretch vibration (υ(C–C) at 1013 and 1580 cm^{-1}, υ(N–C) at 1204 cm^{-1}) are found. Most striking is the intensity decrease of the out-of-plane torsion modes of the phenyl rings (τ(C–C)) at 705 and 877 cm^{-1} in the off-specular spectrum, indicating that their intensities originates mostly from dipole scattering in the specular spectrum. The strong dipole activity of the phenyl ring torsion modes points towards a preferential orientation of the TBI in which the phenyl rings are orientated parallel to the Au(111) surface, *viz.* a planar (*trans*)-geometry, since in this orientation these modes have a strong dipole moment change upon vibration perpendicular to the surface. This interpretation is supported by STM measurements, which show that in the low-coverage regime TBI forms well-ordered islands with the molecules adsorbed in a planar configuration [108].

In the following we investigate the influence of the substrate temperature on the geometrical structure of 1 ML TBI adsorbed on Au(111). Figure 23 shows HREEL spectra taken after deposition of 1 ML of the TBI and subsequent annealing steps to 317, 380 and 440 K. The HREEL spectra of the *trans*-TBI are dominated by the intense phenyl ring torsion located at 230, 703, and 880 cm^{-1} up to heating temperatures of 380 K, due to the planar adsorption geometry. After heating the sample to 440 K a very

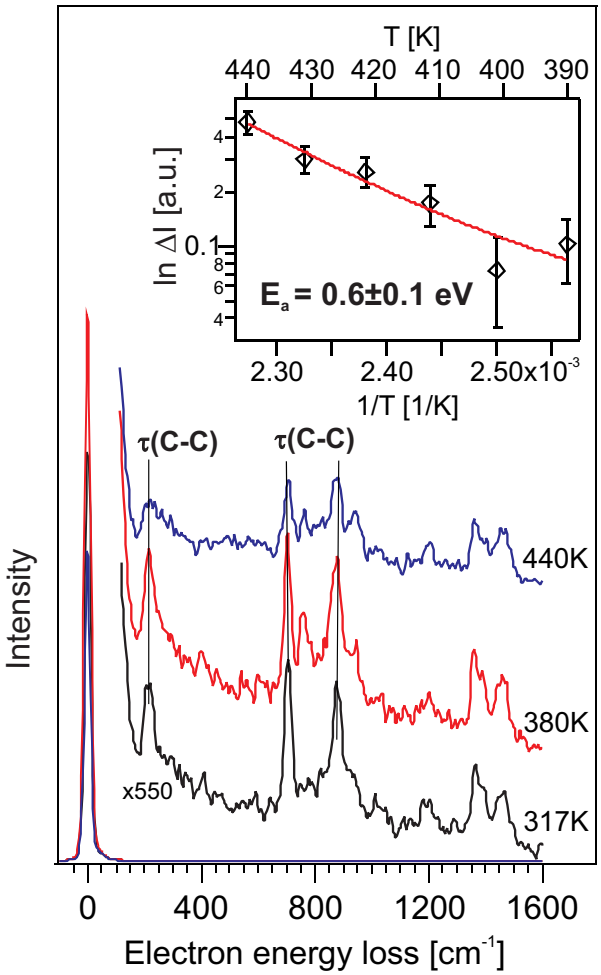

Figure 23. HREEL spectra of 0.5 ML TBI on Au(111) deposited at a substrate temperature of 100 K and after annealing at different temperatures, recorded in specular scattering geometry with a primary electron energy of 3.5 eV. The sample was heated for 2 min at the given temperatures, using a heating rate of 1 K/s, and subsequently cooled down to 100 K. Inset: Intensity change of the phenyl ring torsion mode at 705 cm^{-1} as a function of the substrate temperature. The activation energy (E_a) for the thermally induced *trans* to *cis* isomerization of TBI on Au(111) was obtained by using the Arrhenius expression to fit the data.

strong intensity decrease of theses vibrational modes is observed, which we assign to a conformational change to *cis*-isomers with one phenyl ring pointing upwards, in analogy to the HREEL data of the *trans* to *cis*-isomer of TBA on Au(111) [62]. Note that the spectral changes are not caused by a reduced TBI coverage, since thermal desorption spectroscopy shows basically no desorption at these conditions. Therefore we assign the observed changes to a thermally activated *trans* to *cis* isomerization of TBI on Au(111), which has also been supported by STM measurements [108].

In order to gain a quantitative insight into the activation barrier governing the thermally induced *trans* to *cis* isomerization, we studied the changes in the vibrational loss intensities during the *trans* to *cis* transition. Specifically, intensity changes of the

phenyl ring torsion modes at 703 and 875 cm^{-1}, were used as a quantitative measure for the reaction. The activation energy ($E_{a)}$ is determined from the relative change ΔI in peak intensity ($\Delta I = (I_0 - I_i)/I_0$) between the *trans* TBI covered surface at 317 K and the same surface annealed at a particular temperature, using the Arrhenius-like expression $\Delta I = I_p exp(-E_a/k_B T)$ (with I_p an intensity factor and k_B the Boltzmann constant [164]). From these measurements, we derive a value of 0.6±0.1 eV for the activation energy (see inset of Figure 23). In comparison, the calculated barrier between the stable *trans* and the metastable *cis* form for free imine derivatives in solution is around 1 eV [162]. Thus, we find a barrier reduction of about 0.4 eV for the surface-bound TBI, indicating that the potential energy landscape is significantly different from that in the free molecule. Moreover, at the surface, the *cis*-isomer turned out to be the energetically more stable species, reversing the situation known for the TBI in the liquid phase, as schematically shown in Fig. 24. While the *trans*-TBI molecules interact rather

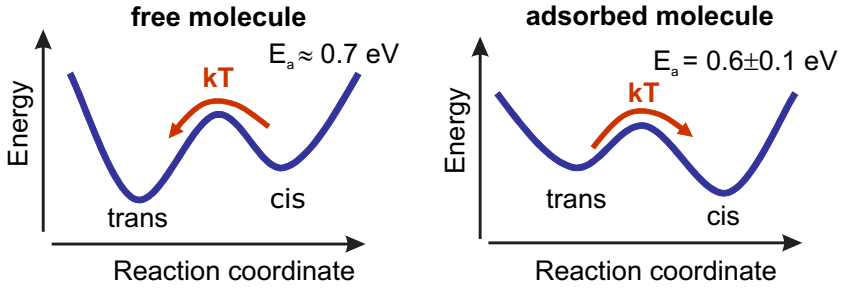

Figure 24. Scheme of the double potential well for the *trans* and *cis* isomer of TBI in solution (free molecule) and adsorbed on Au(111), respectively.

weakly with the Au(111) surface (due to the *tert*-butyl legs) this might be different when they are in the *cis*-state because the lone pair electrons of the N atom can eventually reach the metal surface. A possible chemical interaction could be a σ-bond of the lone pair electrons with the metal substrate, similar to the complexation of metal atoms with imine compounds [165]. The observed inverted thermal isomerization behavior could be due to such an increased coupling to the surface as well as to a modified potential landscape and thus (de)stabilization of certain configurations with respect to the free molecule in solution [108].

To explore the reversibility of the thermally activated *trans* to *cis* reaction process, illumination experiments were performed in order to drive the back reaction (*cis* to *trans*). We illuminated the sample with continuous wave laser diodes at wavelengths of 405 and 445 nm. However, no reduction of the *cis* species and thus an evidence for a back-switching of the *cis* TBI molecules was found in HREEL spectroscopy as well as in STM imaging [108]. This could be a result of the above-mentioned chemical interaction with the surface.

Note that light exposure with varying photon doses at 355 and 445 nm (3.5 and 2.8 eV), respectively, of 1 ML TBI in its trans-configuration adsorbed on Au(111) provoked no changes in the vibrational structure, *viz.*, no modification of the adsorption geometry

is observed. We propose that the photoisomerization is suppressed for coverages ≤ 1 ML. Presumably, this arises from the strong electronic coupling between the molecules and the metallic substrate leading to ultrashort lifetimes of molecular excited states.

3.5. Photoisomerization ability of tetra-tert-butyl-stilbene on Au(111)

Among azobenzenes, Stilbene and its derivatives are one of the most studied classes of photochromic systems [18, 19, 20, 3]. They undergo a reversible photoinduced *trans/cis*-isomerization through the rotation around the C=C double bond due to a $\pi \rightarrow \pi^*$ transition. In contrast to azobenzenes the thermal activated back reaction (*cis* $\rightarrow$ *trans*) is impossible due to a high activation barrier of around 1.9 eV.

Beside studies on the adsorption behavior of stilbenes adsorbed on Cu(110) [166], Si(100) [167] and Ag/Ge(111)-$\sqrt{3}$ [168, 169], respectively, photoinduced *trans/cis*-isomerization of the parent unsubstituted stilbene on Ag/Ge(111)-$\sqrt{3}$ has been analyzed by scanning tunneling spectroscopy [170, 60]. Thereby a biexciton-assisted photoisomerization model has been proposed in order to explain the optically-induced conformational change of stilbene pairs. Contrary, no photoisomerization of stilbene adsorbed on $Al_2O_3(0001)$ has been observed [171].

By employing HREELS and 2PPE we studied the adsorption geometry and the electronic structure of TBS adsorbed on Au(111). In the low-coverage regime ($\leq$ 1ML) TBS adsorbs in the planar (*trans*)-configuration similar to TBA/Au(111). In contrast to surface-bound TBA no changes in the vibrational or electronic structure due to light exposure are observed. Thus, the photoisomerization ability of adsorbed TBS is quenched. This is presumably caused by a different electronic coupling strength between the TBS and the Au(111) surface in comparison to TBA or due to a repression of the rotational pathway [109].

In order to gain insights into the excitation mechanism, i.e., dipole- versus impact-scattering, and to analyze the adsorption geometry of TBS on Au(111) we performed angular dependent measurements. Figure 25 shows a comparison of HREEL spectra recorded in specular and 9.2° off-specular geometries for 1 ML TBS adsorbed on Au(111). For a detailed assignment of all vibrational modes see Ref. [109]. The huge intensity decrease of the out-of-plane torsion mode of the phenyl rings (τ(C–C)) at 693 cm^{-1} and the C–H bending mode (γ(C–H)) at 861 cm^{-1} in the off-specular spectrum indicates that their intensity originated mostly from dipole scattering in the specular spectrum. The strong dipole activity of the phenyl ring torsion and C–H bending modes points towards a preferential orientation of the TBS parallel to the Au(111) surface, *viz.* planar (*trans*)-geometry, since in this orientation these modes have a strong dipole moment change upon vibration perpendicular to the surface. Moreover, the in-plane modes of TBS, e.g. the stretch vibration of the phenyl rings at 1246 and 1595 cm^{-1} of condensed TBS observed with high intensities, are absence or barely visible in the HREELS of the adsorbed species. This corroborates the proposed planar adsorption geometry. In addition, STM measurements show that in the low-coverage regime TBS

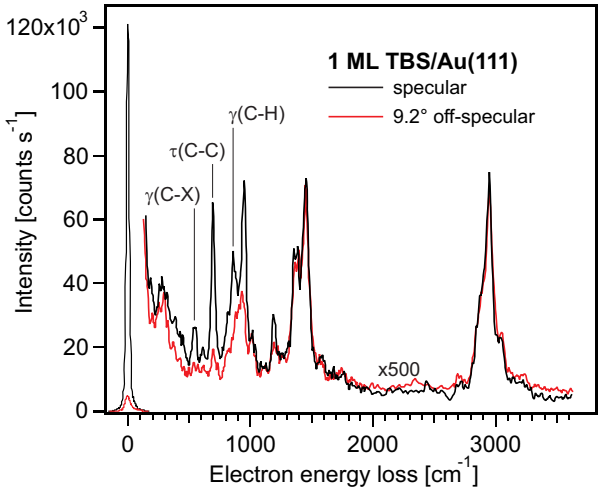

Figure 25. HREEL spectra of 1 ML TBS adsorbed on Au(111) recorded in specular and 9.2°off-specular scattering geometry, respectively, with a primary electron energy of 3.7 eV. Note that C–X stands for the phenyl ring-ethylene bond (reproduced from Ref. [109]).

forms well-ordered islands with the molecules adsorbed in the planar configuration [172].

Illumination experiments have been performed without observable changes in the vibrational structure in the HREELS spectra of TBS/Au(111). Additionally 2PPE measurements have been carried out using different optical excitation energies ranging from 2 – 4.5 eV, in which no light induced changes in electronic structure of surface-bound TBS are observed [109]. Accordingly, we propose that photoisomerization in TBS is suppressed.

For comparison, in TBA/Au(111) the excitation mechanism for molecular switching has been identified to arise from a substrate-mediated charge transfer process, *viz.* the formation of a positive ion resonance. Thereby excitation with photon energies above ≈ 2.1 eV leads to the generation of hot holes in the Au *d*-band, which rapidly relax to the top of the *d*-band and subsequent hole transfer to the HOMO level of TBA inducing the isomerization. Surprisingly the electronic structure of TBS/Au(111) is almost identical to the one of TBA/Au(111). The HOMO level of TBS is located at -1.75 eV with respect to E_F , i.e., at a similar energetic position as the HOMO level of TBA on Au(111), which is -1.85 eV [109]. One may speculate if the overlap between the Au *d*-bands and the HOMO of TBS and thus the electronic coupling is weaker compared to TBA and therefore a transfer of photoexcited Au *d*-band holes to the HOMO of TBS is unlikely. However, based on the mechanism for the photoinduced isomerization of TBA on Au(111), it is evident that a (strong) electronic coupling must be existent, i.e., some degree of hybridization between the Au *d*-band and the HOMO of TBA, presumably *via* the N=N bonding or the lone pairs at the nitrogen.

In addition it is an open question if the cationic state of TBS would stimulate a conformational change. Quantum chemical calculations of the potential energy surfaces for the free TBA and TBS molecule corroborate this conclusion. They indicate that for

the TBA cation larger gradients at the Franck-Condon point than for the TBS cation are exist. Furthermore in the cationic states the barrier is strongly reduced in TBA compared to TBS [109]

4. Ring opening reaction in spiropyran

Beside the *trans/cis*-isomerization, the ring opening and ring closure reaction is the main reaction pathway of photochromic systems. Nitro-substituted spiropyran is an example, which undergoes such a photoinduced reaction between the closed spiropyran (SP)-form and open merocyanine (MC)-isomer (see Figure 26). The SP $\rightarrow$ MC transformation follows a multi-step pathway, thereby the dissociation of the spiro C–O bond is the rate-determining step [173], provoking both a complete change of the molecular structure and a redistribution of charge. Whereas spiropyran is three-dimensional, inert and colorless, the merocyanine is planar, highly reactive, colored, conjugated, and it possesses a large dipole moment due to the stabilization of a zwitterionic form. Apart from the reversible

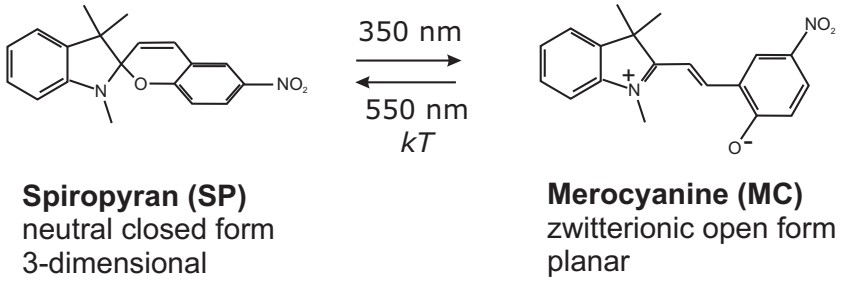

Figure 26. Structure of the trimethyl-6-nitro-spiropyran (SP) and one of its merocyanine (MC) zwitterionic isomers.

photoinduced reaction between both isomers a thermally activated reaction is also possible. Thereby the merocyanine isomer is thermally unstable at room temperature and undergoes a back reaction to the more stable closed-form on a time scale of seconds to minutes [174]. Several strategies have been employed in order to balance the thermodynamical equilibrium towards the open isomer. For example, chelation by metal ions at the indole moiety inhibits the ring closure of the MC isomer [175], but allowing the back reaction by photodetachment of the metal cations [176]. In addition, tuning the polarity either of the solvent or *via* molecular substituents can also retard the thermal back reaction of merocyanine [174].

STM studies show that spiropyran molecules adsorbed on Au(111) form well-ordered structures [177, 178]. Photoinduced or thermally activated ring opening and ring closure reactions of spiropyran at metal surfaces have not been investigated so far. Only photo stimulated switching in thick films adsorbed on MgO(100) has been observed [179].

Using HREELS we demonstrate that trimethyl-6-nitro-spiropyran molecules undergo a thermally induced ring opening reaction (SP $\rightarrow$ MC) when adsorbed on a

Au(111) surface. We find that the reaction proceeds completely in a narrow temperature window right above room temperature and follows similar dissociation pathways as in solution, namely the dissociation of the C–O bond, followed by the relaxation into planar MC conformers. However, on the gold surface the reaction is complete and the conjugated open form turns out to be more stable, reversing the situation usually found in solution. Contrary to the thermally activated ring opening reaction of spiropyran adsorbed on Au(111), a photoinduced ring opening reaction of the adsorbed molecules using different photon energies (355, 405, 445 nm) is suppressed, i.e., no changes in the vibrational structure are observed, presumably due to the ultrashort lifetime of the molecular excited states.

4.1. Thermally activated ring opening reaction

STM studies by Pascual and coworkers [164] show that spiropyran deposited on a cold Au(111) surface undergoes an ordering transition at a temperature of $\approx$ 240 K leading to the formation of extended self-assembled domains. The islands are composed of molecular rows, where the molecules alternate their orientation as can be seen in Figure 27 (a). In spite of such an anisotropic structure, the domains show an overall rounded shape, indicating that intermolecular interactions within the layer are of similar strength both along and across the molecular rows. The observation of the unperturbed Au(111) herringbone reconstruction underneath the layers suggests that the molecules adopt a weakly bonded adsorption state. High resolution STM images show that all molecules exhibit the same shape and orientation on the surface demonstrating that only one type of molecular species is existent (see inset of Figure 27(a)). Annealing the sample to $T_{ann} \approx 300$ K changes the properties of the molecular layer drastically. The two-dimensional molecular domains disappear, and a new phase composed of molecular chains is observed (see Figure 27(b)). The chains show a preference to follow the underlying Au(111) herringbone reconstruction, as well as to avoid lateral packing, even in the case of higher coverages. The former can be understood as a consequence of an enhanced interaction with the metal surface. The latter is characteristic of long-range repulsive interactions among chains, similar to those found in ensembles of organic molecules with large dipole moments or charge transfer on metal surfaces [180, 181, 182]. Hence, a stronger interaction of the high-temperature phase with the metal surface can be concluded by the STM observations.

Based on the isomerizable structure of spiropyran, one may associate the two observed phases with structures formed each by solely one of the two different isomers of the parent spiropyran compound, with a complete transition from one to the other triggered by temperature and by the presence of the metal substrate. However, the STM images neither provide a definitive assessment of the molecular isomers, nor their orientation, which appear at each phase. In order to identify them, we performed HREELS as a function of the annealing temperature.

Figure 28(a) shows the HREEL spectra of $\approx$ 0.7 ML spiropyran/Au(111) annealed

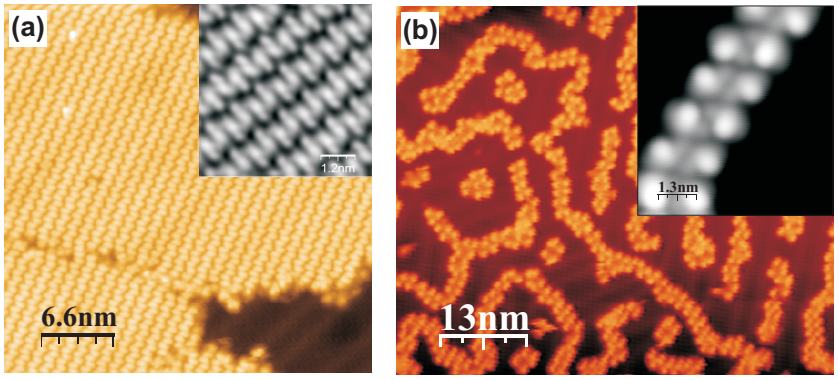

Figure 27. (a) STM image of the spiropyran-covered Au(111) surface annealed to $T_{ann} \approx 240$ K. The height of the molecular islands oscillates around 0.3±0.1 nm depending on the applied sample bias. Inset: High resolution STM image showing the alternating alignment of molecules along rows and their intramolecular chiral structure. The unit cell indicated as a dashed rectangle amounts to 1.2 ± 1.1 nm^2 (I_t=4.0 pA, V_s=1.0 V). (b) STM image of an adsorbate-covered Au(111) surface after annealing to temperatures above $T_{ann} \approx 305$ K (I_t=20 pA, V_s=1.1 V). Inset: High resolution STM image of the molecular chains showing that the molecular species exhibit an intramolecular pattern composed of a 0.1 nm high planar oval structure with a 0.25 nm high internal lobe (I_t=50 pA, V_s=1.0 V). All STM images are reproduced from Ref. [164].

to a substrate temperature of 240 K and recorded in specular and 9.2° off-specular scattering geometries in order to analyze the adsorption geometry. In the specular spectrum several vibrational features are detected, here we discuss only the vibrational modes which are relevant for both the identification of the isomers, i.e., SP or MC, and the determination of the adsorption geometry (for the detailed assignment of all vibrations see Ref. [164]). Strong vibrations of the phenyl ring torsion (out-of-plane, τ(C–C) at 492 and 844 cm^{-1}), C–H deformation (out-of-plane, γ(C–H) at 753, 844, and 927 cm^{-1}) as well as C–C stretch (ν(C–C) at 1273, 1473, and 1492 cm^{-1}) and C–C deformation (in-plane, δ(C–C) at 1369 cm^{-1}) modes are observed. None of these modes shows a particular strong dipole activity, indicating that the closed-form (spiropyran) is existent, where one phenyl ring is orientated parallel and the other one perpendicular to the surface. In addition, the appearance of the butterfly torsion mode between the pyran and phenyl ring ($\tau_{butt.}$ at 256 and 279 cm^{-1}) and the O–C–N stretch vibration (ν_s(O–C–N) at 947 cm^{-1}) clearly points towards the closed-form. Since the C–N (1273 cm^{-1}) and the N–CH_3 stretch (1311 cm^{-1}) vibrations show high intensities and the symmetric and asymmetric stretch modes of the NO_2-group, which are located around 1336 and 1515 cm^{-1}, respectively, are absence we propose an adsorption geometry in which the benzopyran moiety is orientated parallel and the indoline unit perpendicular to the surface. Note that in the case of a perpendicular orientation of the benzopyran unit one would expect an intense NO_2 stretch vibration due to a high dipole activity.

Annealing the sample to 323 K results in significant changes in the vibrational structure as can be seen in Fig. 28(b). The contributions of the C–C stretch and C–C

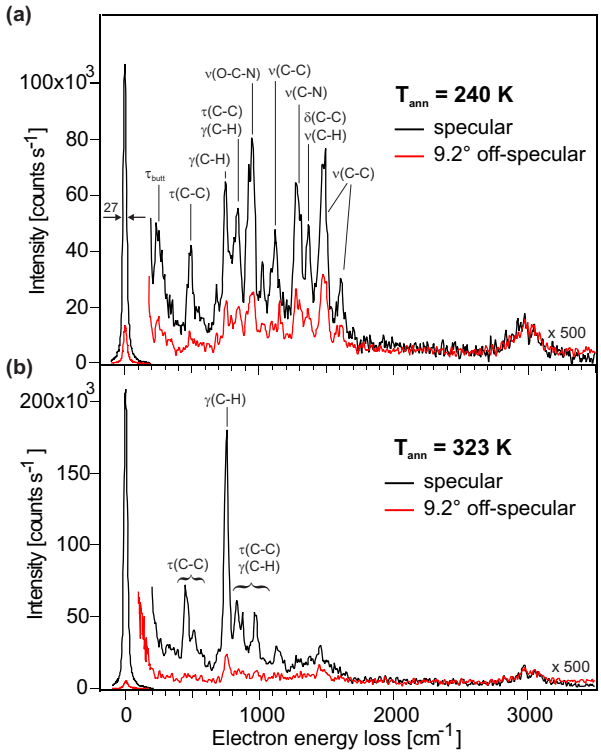

Figure 28. HREEL spectra of 0.7 ML SP adsorbed on Au(111) annealed to a) T_{ann}= 240 K and b) T_{ann} = 323 K. The spectra are recorded in specular and 9.2° off-specular scattering geometries with a primary electron energy of 3.7 eV (reproduced from Ref. [164]).

deformation modes are suppressed, whereas the C–C torsion and the C–H deformation vibrations strongly gain intensity. Moreover the butterfly torsion mode and the O–C–N stretch mode are missing. We interpret these drastic changes to be caused by a thermally induced ring open reaction. The strong dipole activity of the phenyl ring torsion and the C–H deformation modes clearly indicates a parallel orientation (flat lying) of the merocyanine with respect to the surface (see Fig. 29). Furthermore, the flat lying adsorption geometry of the merocyanine obviously leads to a more homogeneous film, resulting in a smaller scattered elastic electron beam (reduced diffuse scattering), which causes an increase in the elastic beam intensity by a factor of two compared to the intensity of the spiropyran-covered surface. Figure 29 shows schematically the

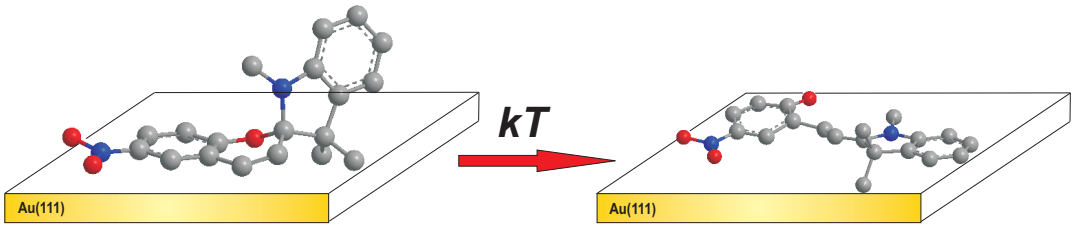

Figure 29. Scheme of thermally activated ring opening reaction of three-dimensional spiropyran (SP) leading to the planar merocyanine (MC) form.

adsorption geometry of the closed three-dimensional spiropyran and planar merocyanine, which can be obtained by a thermally activated ring opening reaction. Note that a thermally driven ring closing reaction even at higher temperatures is suppressed thus the open MC isomer possess a higher stability on the gold surface. The origin of the higher stability of the MC isomer on a gold surface may follow from either the softening of the C-O bond, resulting in a reduction of the activation energy for its dissociation or/and from a larger adsorption energy of the open isomer.

4.2. Kinetics of the bond dissociation

In order to obtain a quantitative insight into the activation barrier governing the ring opening reaction we have performed an analysis of the reaction kinetics using the changes in the vibrational spectra during the SP→MC transition. Since the amount of MC

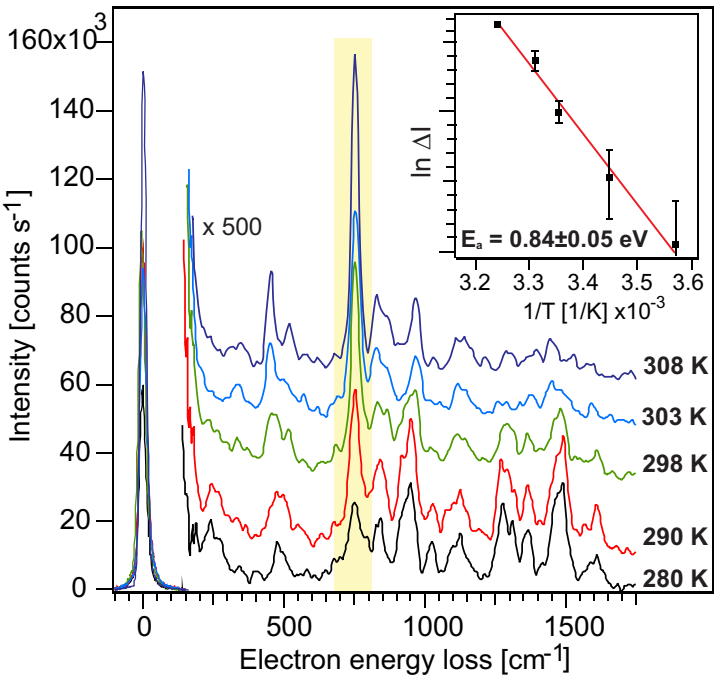

Figure 30. HREEL spectra of 0.7 ML of SP molecules deposited on Au(111) as a function of annealing temperature. The spectra are recorded in specular scattering geometry with a primary electron energy of 3.7 eV. The SP → MC reaction causes a gradual increase in the intensity of the out-of-plane CH bending mode at 754 cm^{-1} (shadowed). Inset: Relative intensity change of this mode as a function of the substrate temperature. The activation energy (E_a) for the ring-opening reaction of spiropyran on Au(111) can be obtained by using an Arrhenius-like expression (see Eq.4) (reproduced from Ref. [164]).

isomers as a function of the annealing temperature is unknown, we used the change in intensity of the C–H-deformation mode at 754 cm^{-1}, which shows the largest change upon ring opening, as a quantitative measure for the reaction (see Fig. 30). Thereby, we determined the activation energy E_a by analyzing the relative change in peak intensity (ΔI) between the SP-covered surface (at 240 K) and the substrate annealed

to a particular temperature, and relating the peak height change to an Arrhenius-like expression

$$\Delta I = I_0 \, exp\left(-\frac{E_a}{k_B T_{ann}}\right) \tag{4}$$

where I_0 is saturation intensity at infinite temperature and k_B is the Boltzmann constant. Note that the measurements were done for equal annealing times (10 minutes) at the particular temperature in each case on a freshly prepared film. From these measurements we derive a value of 0.84 ± 0.05 eV for the activation energy (see inset of Figure 30). This value is surprisingly close to the activation energy for the reaction in solution (≈ 1 eV, depending on the solvent [174]), which can be attributed to the weakly adsorbed state of spiropyran on Au(111).

If the presence of a metal surface does not reduce the barrier for C–O-bond cleavage significantly, it may still balance the energetics towards the merocyanine isomer if an additional mechanism contributes to the stabilization of this form on the surface. The larger interaction of MC molecules with the Au(111) surface, observed by STM, could well play such stabilizing role. The planar conjugated structure of the MC form is prone to interact with electronic states at the metal surface, thus hindering the back reaction. Furthermore, X-ray photoelectron spectroscopy (XPS) and NEXAFS results suggest that the adsorbed merocyanine molecules exist in their zwitterionic form [164]. The large electrical dipole of this form is expected to interact with the metal through the creation of image charges, increasing the strength of the metal-molecule bond.

4.3. Ring-opening/closure reaction ability: electronic structure changes as a probe

Since the geometrical rearrangement of the nitro-spiropyran molecules during the thermal activated ring-opening reaction is very pronounced, it is expected that also fundamental changes in the electronic structure occur when the molecules are switched. For instance, the planar open MC form exhibits a conjugated π-electron system in contrast to the three-dimensional closed SP. However, the molecules in both their open and closed form in direct contact with a metal surface possess clear differences in their respective electronic structure (see Fig. 31 [183]) allowing to discriminate precisely between the two forms and accordingly to follow a potential ring-opening/closure reaction by using 2PPE or scanning tunneling spectroscopy (STS).

Illumination experiments of the SP-covered Au(111) with various wavelength and photon doses followed by 2PPE and STS measurements showed no changes in the electronic structure. Thus no ring opening reaction occurred. The suppression of a photoinduced ring-opening indicates that all potential excitation channels at metal surfaces such as (i) the direct intramolecular electronic (HOMO-LUMO transition) [110, 153] known for the molecules in solution, (ii) the creation of a negative ion resonance (NIR) through an optically induced electron transfer from the metal to the molecules (see below) and (iii) the creation of a positive ion resonance via hole transfer between the metal and the adsorbate [106, 107] are not efficient.

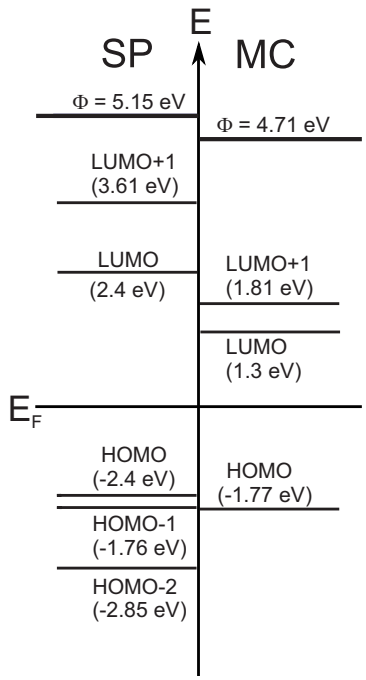

Figure 31. Summary of the molecule-derived electronic states of surface-bound spiropyran in its closed (SP) and open (MC) form as observed in the 2PPE and STS experiments. All energies are referenced to the Fermi level of the Au(111) surface. Φ denotes the work function as determined by 2PPE.

A further approach to stimulate a reaction in SP/Au(111) is the utilization of the STM-tip as an external stimulus [183]. Indeed, using tunneling electrons drives the ring-opening reaction. Figure 32 shows an example of an electron induced SP → MC isomerization at the border of a densely packed molecular island. The bias voltage is increased at a fixed tip-molecule distance while the current (not shown) and the dI/dV signal are recorded (Fig. 32 (b)). When the bias voltage exceeds the LUMO resonance at ≈ 2.2 V a sudden drop in the dI/dV signal indicates a change in the molecule underneath the tip. The following dI/dV spectrum shows that the SP's LUMO has disappeared and a pronounced resonance with a double peak structure characteristic of the LUMO/LUMO+1 double peak of the MC isomer appears. The corresponding STM image (Fig. 32(c)) also shows a change in the topography of the molecule. We interpret this behavior as a switching event induced by electrons resonantly tunneling from the STM tip into the LUMO creating a NIR. The possibility to induce a switching via resonant tunneling into the LUMO has also been proposed in the case of the *trans/cis*-isomerization of azobenzene adsorbed on Au(111) [64]. In contrast to the ring-opening reaction stimulated by the generation of a NIR each attempt to trigger the back-reaction of MC to SP using the STM-tip failed. The same applies for a photoinduced process.

An estimation of the quantum yield by tunneling electrons in an energy range of 1.7 to 2.4 eV leads to $(2.2 \pm 0.2) \cdot 10^{-10}$ events/electron. Compared to the upper limit of a quantum yield that we could have detected in our illumination experiments, this is even one order of magnitude lower. The reason for being able to detect such small

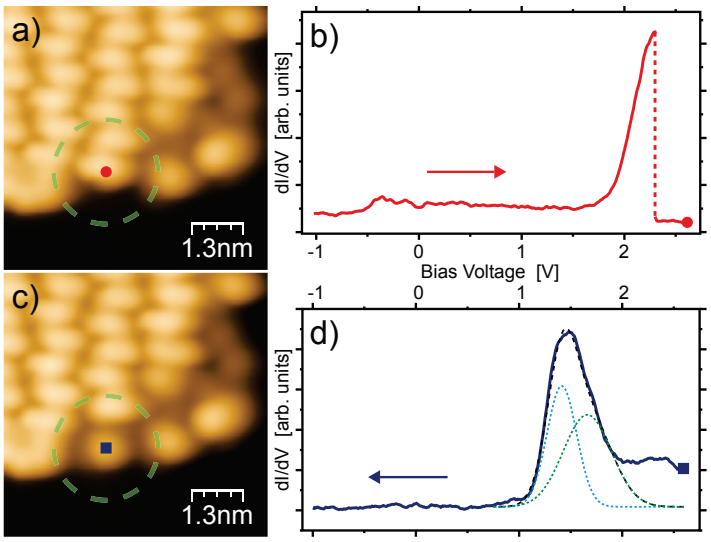

Figure 32. Isomerization of a single molecule induced by electron tunneling. (a) shows parts of an ordered SP island where an scanning tunneling spectrum was taken (b) at the indicated spot. (c) shows the same area on the surface after the switching event and in (d) another STS spectrum taken at the switched molecule is shown (reproduced from Ref. [183]).

quantum yields by electrons is their high tunneling rate, which makes this experiment much more sensitive to such low switching efficiencies. Since the ring-opening reaction toward the open MC form is possible by attaching electrons to the SP LUMO in the STM junction, one would expect that a photoexcited electron transferred from the metal substrate to the LUMO of SP would cause the same effect. This photoexcitation may be resonant, e.g., from the substrate surface state or *via* hot electrons tunneling into the LUMO creating a NIR. Photoswitching may hence be possible but the detection by counting MC molecules is less sensitive than the detection method in electron tunneling spectroscopy. On the other hand, the efficiency to attach an electron to the LUMO is much higher in the STM-junction compared to the indirect way *via* optically excited substrate electrons.

Hence, in comparison to molecules in solution photoinduced switching is effectively quenched on the metal surface. At metal surfaces the lifetimes of excited states are ultrashort, i.e., in the range of femtoseconds as shown for different adsorbates [40, 41, 42, 43, 44], thus not allowing for nuclear motion. Therefore competition between the required nuclear motion and quenching of excited states provides a challenge to realize photoinduced molecular switching at metal surfaces. In addition, steric hinderance effects may play a role, since the molecules lose the freedom to change conformation if the atomic motion is constrained by the surface. Due to the zwitterionic character of MC a strong electronic coupling between the molecules and the substrate exists. Therefore lifting of a molecular unit, e.g. a substituted phenyl ring, allowing the ring closure reaction would require a strong driving force. Additionally, a directed molecular motion is needed allowing the creation of the C–O-bond in order to generate

the closed SP form.

5. Reversible isomerization of an azobenzene functionalized self-assembled monolayer

While in the previous chapters we investigated molecular switches in direct contact with the metallic substrate in a "horizontal" adsorption geometry, in this section we study the switching behavior of azobenzenes incorporated into a self-assembled monolayer (SAM), which are covalently attached *via* anchoring groups to a gold surface. Thus the switches adopt a more or less vertical adsorption geometry with respect to the surface depending on the anchor/linker system. As described in the introduction, for the *trans*- to *cis*-isomerization of an azobenzene functionalized SAM a free volume to prevent steric hinderance is required. In order to provide this we used a tripodal linker system with an adamantane core (see Fig. 33), which covers a surface area whose diameter exceeds that of the functional azobenzene unit. Recently, these kind of three-dimensional linkers with a tetrahedrical core unit for sufficient control of the perpendicular shape and head group to surface distance have been developed [184, 185, 186]. It has been shown that these linker systems equipped with an azobenzene moiety allow photoisomerization when the system is immobilized on a Au(111) surface or applied as an atomic force microscope tip [187], but so far it has not been proven in a SAM.

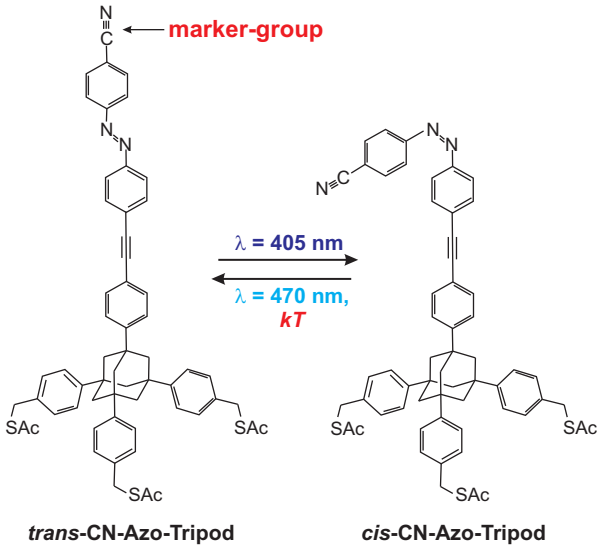

Figure 33. Structure of the *trans*- and *cis*-isomer of the azobenzene derivative considered in this study.

Using sum-frequency generation (SFG) vibrational spectroscopy we studied the photoisomerization of an azobenzene-functionalized SAM in which the azobenzene unit is connected to a tripodal linker system. The linker system is sufficient to yield the free volume thus allowing the photoinduced switching. The azobenzene carries an additional cyano-group (–C≡N) in *para*-position of the phenyl ring which acts as a marker-group

for SFG and permits a direct measure of the switching state (see Fig. 33).

We will demonstrate that SFG is a suitable tool to determine the reversible photoinduced *trans/cis*-isomeriztaion of an azobenzene-functionalized SAM [188]. Optical excitation at 405 nm leads to a *trans* → *cis* conformational change while the back reaction (*cis* → *trans*) occurs at a wavelength of 470 nm. As these excitation wavelengths correspond to the one used for the free molecules in solution, we propose that the photoisomerization is driven by a direct (intramolecular) electronic excitation. This is expected since the tripodal linker system should result in a weak interaction between the azobenzene unit and the Au substrate.

5.1. Adsorption of the azobenzene-functionalized SAM

In order to determine the switching state of the azobenzene-functionalized SAM by SFG the azobenzene unit was synthesized with a C≡N-marker group in *para*-position of the phenyl ring (see Fig. 33). In most cases the C≡N-stretch vibration results in a strong signal intensity and is known to be in the range between 2260 and 2200 cm^{-1}, thus in a frequency window where vibrations of air constituents like H_2O or CO_2 and C–H modes do not interfere. Figure 34(a) shows a SFG spectrum of the azobenzene-functionalized SAM in the frequency region between ≈ 2100 and 2350 cm^{-1}.

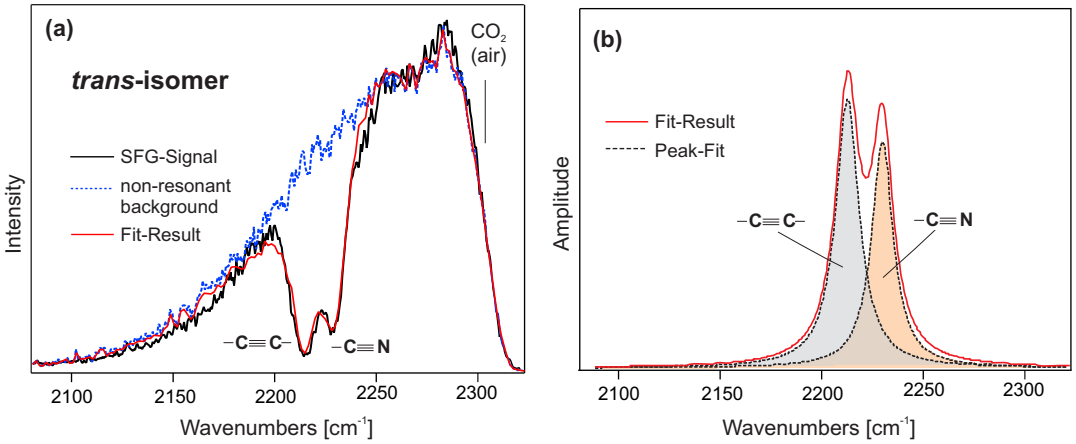

Figure 34. (a) Broadband-IR-VIS-SFG spectrum in the frequency region of the C≡C- and C≡N-stretch vibrations of the azobenzene-functionalized SAM. Also shown is the non-resonant background measured from the bare Au-substrate and a fit using two Lorentzian resonances (see eq. 2), which nicely models the experimental data. The lineshape in the resonance region originate from the relative phase of the vibrational resonance with respect to the nonresonant contribution. Around 2349 cm^{-1} the asymmetric CO_2 stretch vibration in air adsorbs all IR intensity. (b) Lorentzian fits of the vibrational resonances result in a ratio of the amplitudes between the C≡C- and C≡N-modes of 1:0.87 (reproduced from Ref. [188]).

Two strong vibrational features are observed, which can be assigned to the C≡C- and C≡N-stretch vibrations located at 2215 and 2228 cm^{-1}, respectively. Above ≈ 2325 cm^{-1} the asymmetric CO_2 stretch vibration in air absorbs all IR intensity. In addition,

a fit using two Lorentzian resonances (see eq. 2) and the non-resonant background from the bare Au substrate which is proportional to the IR intensity are shown. The fit nicely reproduces the measured SFG-spectrum. The lineshape of the SFG signal strongly depends on the relative phase ϕ_q of the vibrational resonances with respect to the nonresonant contribution. In the case of the C≡C- and C≡N-stretch mode ϕ_q is $3/4\pi$ and $1/2\pi$, respectively, thus leading to a SFG signal which looks apparently similar to an IR absorption spectrum. Figure 34(b) displays the two Lorentzian resonances obtained from this fit, which exhibit a ratio of the amplitudes between the C≡C- and C≡N-modes of 1:0.87. Due to the vanishing electric field components of the incident IR-light parallel to the metal surface only vibrations with a component of the dipole moment change normal to the surface are observable. Therefore the appearance of the intense C≡C- and C≡N-vibrational signals points towards a preferential orientation of the azobenzene-linker conjugate perpendicular or nearly perpendicular to the surface in which the azobenzene adopts the *trans*-configuration. Note that the *trans*-isomer is known to be the energetically favorable configuration.

5.2. Reversible trans/cis-photoisomerization

In the following we investigate the effect of illumination on the vibrational structure of the functionalized surface. Figure 35 displays the SFG spectrum after illumination of the SAM with $h\nu$ = 405 nm and a photon dose (number of photons, n_p) of $\approx 10^{18}$ cm^{-2}. Light exposure leads to a decrease in the amplitude of the C≡N-mode,

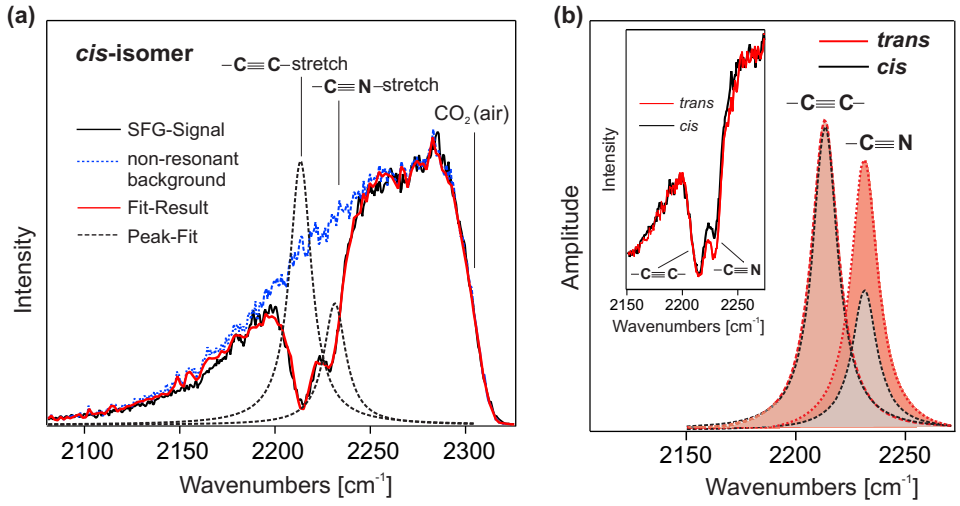

Figure 35. (a) SFG spectrum after illumination of the SAM with hν = 405 nm ($n_p \approx 10^{19} cm^{-2}$). The ratio of the amplitudes between the C≡C- and C≡N-mode is 1:0.46, i.e., the amplitude of the C≡N-mode drops due to the *trans* → *cis* isomerization while the amplitude of the C≡C mode stays constant. (b) Comparison between the fits using Lorentzian resonances before (*trans*-configuration) and after illumination (*cis*-configuration). Inset: SFG raw data before and after light exposure with hν = 405 nm (reproduced from Ref. [188]).

while the amplitude of the C≡C-stretch vibration stays constant (see Fig. 35 (b))

indicating that no radiation damage occurs as well as the orientation of the linker system does not change. The ratio of the amplitudes between both vibrations is 1:0.46, thus the amplitude of C≡N-mode decreases by ≈ 50% compared to the non-illuminated film. We assign the change in the vibrational structure to a photoinduced *trans* → *cis* isomerization of the azobenzene unit. In the *cis*-configuration the CN-group is no longer orientated perpendicular (or nearly perpendicular) to the surface (see Fig. 33), therefore the amplitude of the CN-signal drops.

In order to estimate the relative amount of switched molecules in the SAM and to compare this value with the value for the free molecules in solution one has to discuss to what extent the CN-vibration of the *cis*-isomer might contribute to the measured CN-signal. Thereby two possible scenarios can be considered: (i) the CN-vibrational mode does not contribute to the signal or (ii) does make a contribution. In the first case (i) the CN-group of the *cis*-isomer must be orientated almost parallel to the metal surface, since in this configuration the dipole moment change is parallel to surface. This orientation would be possible if the molecules in their *trans*-form are tilted by ≈ 30° and a change in the orientation between the *trans*- and *cis*-isomer of 120° as in the case of the free molecules. A decrease in the amplitude of the CN-signal of about 50% after illumination indicates that half of the molecules which originally contributed to the CN-signal (*trans*-form) no longer make a contribution. If the *cis*-isomers contribute to the CN-signal (the second case (ii)) then the amount of switched molecules has to be even larger in order to provoke a reduction of 50%. Thus a quantity of ≈ 50% of the *trans*-isomers which undergo a light induced conformational change is the lower limit. For comparison, in the photostationary state the amount of switched *cis*-molecules in the liquid phase is ca. 55% calculated from the intensities of the absorption bands associated with the $\pi \rightarrow \pi^*$ transition in the UV/Vis spectra before (*trans*-isomer) and after illumination at 405 nm.

Since it is known for the molecules in solution that the reverse process, i.e., the *cis* → *trans* isomerization can be stimulated by photoexcitation in the Vis-range, illumination experiments with $h\nu = 470$ nm were performed. Indeed, these measurement indicate that by light exposure at 470 nm ($n_p \approx 6 \cdot 10^{19} cm^2$) the same SFG amplitude of the C≡N mode can be retrieved as from the SAM with the azobenzene in the *trans*-configuration (see Fig. 36). Repeating the light exposure with the two different wavelength of 405 and 470 nm, respectively, demonstrates that the changes in the amplitude of the C≡N-mode are reversible as shown in Fig. 36. We propose that the reversible changes in the vibrational structure are due to a structural change of the SAM, associated with the reversible isomerization process. The 405 nm light induces the *trans* → *cis* isomerization whereas the reverse process (*cis* → *trans*) can be stimulated by 470 nm light. Using the tripodal linker system with the adamantane core, which generates a triangular footprint with a side length around 15 Å [189], allows the reversible isomerization which is associated with a significant structural change due to a sufficient free volume.

To evaluate the underlying mechanism responsible for the photoinduced isomerization of the azobenzene-functionalized SAM, two possible scenarios can be

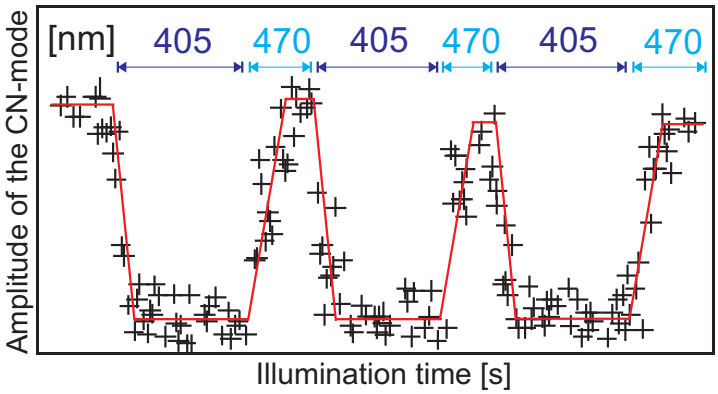

Figure 36. Change in the amplitude of the C≡N signal as a function of illumination with the two different wavelengths (405 and 470 nm), demonstrating the light induced reversible changes in the vibrational structure due to the *trans/cis*-isomerization.

considered, an intramolecular electronic excitation within the adsorbate or a substrate-mediated photochemical process. In the case of the immobilized azobenzene-linker conjugate we propose that a direct optically electronic excitation drives the isomerization, since the tripodal linker system results in a weak interaction between the functional azobenzene unit and the metal substrate, *viz.* the azobenzene is electronically decoupled. Hence, the electronic structure of the adsorbed molecule will be very similar to the molecule in the liquid phase, i.e, the absorption bands should be barely modified. Hence, photoexcitation at 405 nm leads to *trans* $\rightarrow$ *cis* isomerization of the adsorbed molecules, whereas excitation at 470 nm drives the back reaction (*cis* $\rightarrow$ *trans*) analogous to the liquid phase.

5.3. Quantification of the photoinduced isomerization

In order to quantify the light-induced *trans/cis*-isomerization of the azobenzene functionalized SAM on the Au surface we evaluated effective cross sections for both the *trans* $\rightarrow$ *cis* ($\sigma_{eff}(cis)$) and the *cis* $\rightarrow$ *trans* ($\sigma_{eff}(trans)$) reaction. Since the amount of *cis*-isomers as a function of photon dose is unknown, we used the change in the amplitude of the CN-stretch mode as a measure for the switching process, *viz.* we correlated the observed changes as a function of photon dose with the number of switches molecules (see Fig. 37). By using an exponential saturation function one can estimate an effective cross section

$$\Delta A = \Delta A_{\infty}\left(1 - e^{-(\sigma_{eff}\cdot n_p)}\right) \tag{5}$$

where ΔA is the change in the amplitude of the CN-mode, ΔA_{∞} corresponds to the asymptotic change in the CN-amplitude and n_p is the photon dose (number of photons). The solid lines in Fig. 37 represent fits according to eq. 5. From these fits one derives an effective cross section of $\sigma_{eff}(cis) = 4 \pm 1 \times 10^{-18} cm^2$ at 405 nm for the *trans* $\rightarrow$ *cis* isomerization and for the back reaction (*cis* $\rightarrow$ *trans*) a value of

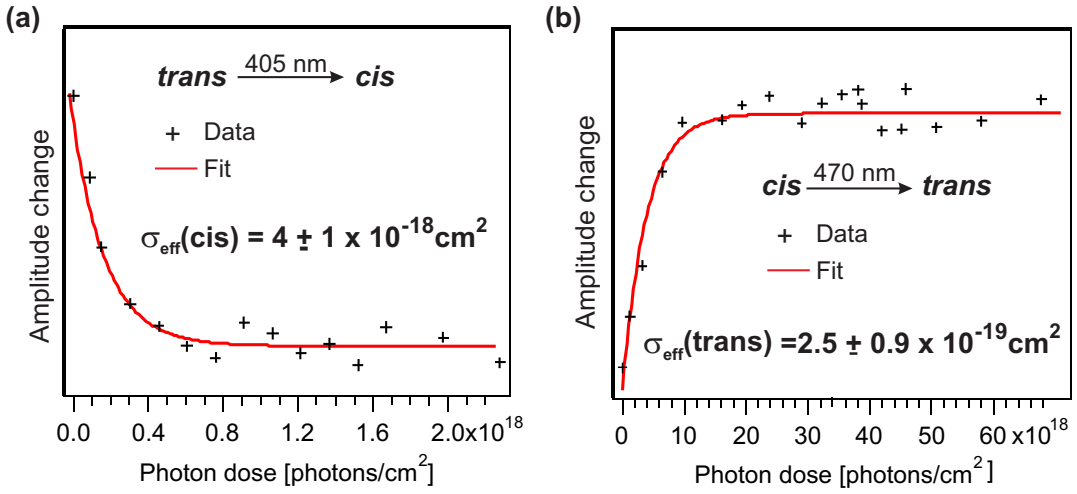

Figure 37. Change in the amplitude of the CN-mode as a function of photon dose. (a) Decrease of the amplitude of the CN-mode as a function of photon dose at $h\nu = 405$ nm due to the *trans* $\rightarrow$ *cis*-isomerization. (b) Increase of the amplitude of the CN-mode as a function of photon dose at $h\nu = 470$ nm due to the *cis* $\rightarrow$ *trans*-isomerization. The solid lines in (a) and (b) represent fits using the exponential saturation function (5) (reproduced from Ref. [188]).

$\sigma_{eff}(trans) = 2.5 \pm 0.9 \times 10^{-19} cm^2$ at 470 nm. The difference between the isomerization cross sections of approximately one order of magnitude might be related to the different absorption cross sections in the UV/vis frequency region. While excitation around 405 nm leads to a strong absorption due to $\pi \longrightarrow \pi^*$ transition, excitation at 470 nm induces a $n \longrightarrow \pi^*$ transition which is symmetry forbidden and therefore a decreased absorption is observed. Under the assumption that the quantity of switched molecules in solution and in the SAM is similar, i.e., ca. 50% (see above) then the photoisomerization cross sections of the azobenzene functionalized SAM closely resemble the one known for azobenzene and its derivative in solution. This reflects the strong decoupling of the functional azobenzene moiety from the metal substrate due to the tripodal linker system with the adamantane core.

6. Conclusion and Outlook

In this work, we have studied the optically and thermally induced isomerization ability of molecular switches adsorbed on noble metal surfaces employing two-photon photoemission (2PPE), high-resolution electron energy loss spectroscopy (HREELS) and sum-frequency generation (SFG) vibrational spectroscopy. Two approaches concerning the surface connection of the molecular switches are utilized: switches in direct contact with the surface (physisorbed or weak chemisorbed, horizontal adsorption geometry) and switches incorporated in a self-assembled monolayer (SAM) which are covalently attached to the substrate by means of anchoring groups (vertical adsorption geometry). For both concepts a successful isomerization has been demonstrated *via* reversible

changes in the electronic and/or geometrical structure of the adsorbed molecular switches, moreover indicating that 2PPE and surface vibrational spectroscopy (HREELS and SFG) are suitable tools to study isomerization reactions at metal surfaces and to obtain detailed knowledge of the underlying elementary processes, for instance the underlying excitation mechanism in the photoinduced isomerization.

We find that in the case of molecular switches directly bound to the metal surface the isomerization properties change significantly in comparison to the free molecules in solution. Thereby the results of a systematic variation of the switching unit (diazo-, imine-, and ethylene-group, spiropyran), the substrate and the electronic structure of the molecular switch, respectively, mirror the delicate balance between the switching ability and the strength of the adsorbate/substrate-interaction. The latter determines the geometrical and electronic structure of the adsorbate and thus the lifetime of molecular excited states.

As shown for tetra-*tert*-butyl-azobenzene (TBA) adsorbed on Au(111) the cross sections (efficiency) for the photoisomerization as well as the amount of switched molecules in the photostationary state are strongly reduced compared to the corresponding quantities in the liquid phase. In addition the activation energy for the thermally driven isomerization (*cis* $\rightarrow$ *trans*) is drastically reduced, indicating that the potential energy landscape of the adsorbed TBA is remarkably different from the free molecule. A suppression of the photoisomerization is observed for most systems (e.g., tetra-*tert*-butyl-imine(TBI)/Au(111), tetra-*tert*-butyl-stilbene (TBS)/Au(111), spiropyran/Au(111)) presumably due to effective quenching processes of molecular excitations or steric hindrance effects, since the molecules lose the freedom to change their conformation if the atomic motion is constrained by the surface. Furthermore in the presence of a metal surface the thermal stability of the molecular switches (spiropyran/Au(111), TBI/Au(111)) can strongly be modified, *viz.* reversing the situation usually found in solution. The mechanism of optical excitation and molecular switching of TBA on Au(111) has been identified to arise from a substrate-mediated charge transfer process, where hot holes from the Au *d*-bands are attached to the adsorbate, creating a transient positive ion, which may subsequently result in the conformational switching of adsorbed TBA. The substrate mediated excitation process for surface-bound TBA is thus completely different from the well-known direct (intramolecular) excitation mechanism operative in the photoisomerization of free molecules. In contrast, we conclude that the optically induced isomerization of molecular switches in the second adsorbate layer (di-methoxy-tetra-*tert*-butyl-azobenzene/Au(111), carboxy-benzylideneaniline/Au(111)) or incorporated in a SAM is driven by a direct (intramolecular) excitation analogous to the molecules in the liquid phase, since the molecular switches are electronically decoupled from the metallic substrate. Moreover, the use of a tripodal linker system with an adamantane core in an azobenzene-functionalized SAM guaranties lateral spacing which enables the reversible photoisomerization. A precise analysis of the adsorption geometry of azobenzene and TBA on Ag(111) using normal incidence X-ray standing wave technique

and corresponding large-scale density-functional theory (DFT) calculations as well as DFT calculations on both molecules adsorbed on Au(111) demonstrate that the photochemically active diazo group in TBA is not decoupled, thus the decoupling concept *via* bulky *tert*-butyl-spacer legs is questionable. The role of the *tert*-butyl groups for the switching ability is therefore more subtle than simple geometric decoupling.

The present results provide examples that demonstrate the feasibility of molecular switching at metal surfaces. However, our study also reveals, that the isomerization properties of surface-bound molecular switches can be very different compared to free molecules, reflecting the strong influence of the interaction with the metal substrate. Since the adsorbate/substrate-interaction and accordingly the adsorption geometry and the electronic structure of the adsorbate play a key role, future studies will concentrate on the controlled variation of the molecule/substrate-interaction. Thereby different approaches like the use of electron-withdrawing or -donating substituents (push-pull systems) and/or different spacer legs (anchor/linker-systems) or thin insulating films may be considered. Systematic studies along these lines may help to optimize the photoisomerization efficiency and to address different excitation mechanisms in a controlled way. Another attractive route of research aims to achieve novel functionalities by cooperative switching processes mediated by adsorbate/adsorbate-interactions in systems where the switching probability of each individual molecule depends on switching state of the neighboring molecules. Such cooperative effects allow to craft switchable patterns in molecular adlayers [46] or to realize logical circuits from molecular building blocks [190]. These examples open the perspective to design functional surfaces, whose molecular properties can be changed at will between various states.

Acknowledgments

It is a great pleasure to thank all persons and institutions who made this work possible. First of all, I want to thank Martin Wolf who supported this study by his scientific insight, systematic approach, and encouragement. I have been fortunate to have had and have excellent Diploma and Ph.D students as well as postdoctoral fellows, namely Christopher Bronner, Anton Haase, Sebastian Hagen, Christian Kördel, Matthias Koch, Felix Leyssner, Isabel Martin, Stephan Meyer, László Óvári, Michael Schulze, and Steffen Wagner working with me in this project. I am grateful for the fruitful collaboration with Katharina Franke, Leonhard Grill, Rainer Haag, Stefan Hecht, Tillmann Klamroth, Wolfgang Kuch, Nacho Pascual, Karsten Reuter, Karola Rück-Braun, Peter Saalfrank, Stefan Tautz, Martin Weinelt, and their coworkers. Funding by the Deutsche Forschungsgemeinschaft through the collaborative research centre Sfb 658 has been essential for this work.

References

[1] W. Gärtner. *Angew. Chem. Int. Ed*, 113:3065, 2001.

[2] V. Balzani, A. Credi, and M. Venturi, editors. *Molecular devices and machines - A journey into the nanoworld*. Wiley-VCH,Weinheim, 2003.
[3] B. Feringa. *Molecular Switches*. Wiley-VCH, Weinheim, 2001.
[4] M.R. Bryce, M.C. Petty, and D. Bloor. *Molecular electronics*. Oxford University Press, New York, 1995.
[5] G. Cuniberti, F. Fagas, and K. Richter, editors. *Introducing molecular electronics*. Springer, Berlin, Heidelberg, 2005.
[6] edited by M. Irie. Special issue: Photochromism: Memories and switches. *Chem. Rev.*, 100:1683, 2000.
[7] K. Uchida, N. Izumi, S. Sukata, Y. Kojima, S. Nakamura, and M. Irie. *Angew. Chem. Int. Ed.*, 45:6470, 2006.
[8] R. Rosario, D. Gust, A.A. Garcia, M. Hayes, J.L. Taraci, T. Clement, J.W. Dailey, and S.T. Picraux. *J. Phys. Chem. B.*, 108:12640, 2004.
[9] N. Katsonis, T. Kudernac, M. Walko, S.J. van der Molen, B.J. van Wees, and B.L. Feringa. *Adv. Mater.*, 18:1397, 2006.
[10] C. Joachim, J.K. Gimzewski, and A. Aviramo. *Nature*, 408:541, 2000.
[11] N. Katsonis, M. Lubomska, M.M. Pollard, B.L. Feringa, and P. Rudolf. *Prog. Surf. Sci*, 82:407, 2007.
[12] T. Hugel, N.B. Holland, A. Cattani, L. Moroder, and H.E. Gaub. *Science*, 296:1103, 2002.
[13] Z.F Liu, K. Hashimoto, and A. Fujishima. *Nature*, 347:658, 1990.
[14] T. Ikeda and O. Tsutsuma. *Science*, 268:1873, 1995.
[15] J. Wachtveitl, S. Spörlein, H. Satzger, B. Fonrobert, C. Renner, R. Behrendt, D. Oesterhelt, L. Moroder, and W. Zinth. *Biophys. J.*, 86:2350, 2004.
[16] Zhang, M.-H. Du, H.-P. Cheng, X.-G. Zhang, A.E. Roitberg, and J.L. Kraus. *Phys. Rev. Lett.*, 92:158301, 2004.
[17] A.C. Whalley, M.L. Steigerwald, X. Guo, and C. Nuckolls. *J. Am. Chem. Soc.*, 129:12590, 2007.
[18] J. Saltiel and Y.-P. Sun. *Photochromism - Molecules and Systems*. Elsevier, Amsterdam, 2003.
[19] D.H. Waldeck. *Chem. Rev.*, 91:415, 1991.
[20] H. Maier. *Angew. Chem. Int. Ed.*, 31:1399, 1992.
[21] N. Tamai and O.H. Miyasaka. *Chem. Rev.*, 100:1875, 2000.
[22] H. Rau. *Photochromism - Molecules and System*. Elsevier, Amsterdam, 2003.
[23] D. Fanghänel, G. Timpe, and V. Orthman. *Photochromism - Molecules and System*. Consultants Bureau, New York, 1990.
[24] M.A. El-Bayoumi, M. El-Asser, and F. Abdel-Halim. *J. Am. Chem. Soc.*, 93:586, 1971.
[25] H.B. Bürgi and J.D. Dunitz. *Helv. Chim. Acta*, 52:1747, 1970.
[26] T.A. Jung, R.R. Schlittler, and J.K. Gimzewski. *Nature*, 386:696, 1997.
[27] F. Moresco, G. Meyer, K.-H. Rieder, H. Tang, A. Gourdon, and C. Joachim. *Phys. Rev. Lett.*, 86:672, 2001.
[28] D. Dulic, S.J. van der Molen, T.Kudernac, H.T. Jonkman, J.J.D. de Jong, T.N. Bowden, J. van Esch, L.B. Feringa, and J.B. van Wees. *Phys. Rev. Lett.*, 91:207402, 2003.
[29] X.L. Zhou, X.-Y. Zhu, and J.M. White. *Surf. Sci. Rep.*, 13:73, 1991.
[30] H.-L. Dai and W. Ho. *Laser Spectroscopy and Photochemistry at Metal Surfaces*. World Scientific, Singapore, 1995.
[31] X.-Y. Zhu. *Annu. Rev. Phys. Chem*, 45:113, 1994.
[32] F.M. Zimmermann and W. Ho. *Surf. Sci. Rep.*, 22:127, 1995.
[33] H. Guo, P. Saalfrank, and T. Seideman. *Prog. Surf. Sci*, 62:239, 1999.
[34] Y. Matsumoto. *Bull. Chem. Soc. Jpn.*, 80:842, 2007.
[35] M.R. Hoffmann, S.T. Martin, W. Choi, and D.W. Bahnemannt. *Chem. Rev.*, 95:69, 1995.
[36] A.L. Linsebigler, G. Lu, and J.T. Yates Jr. *Chem. Rev.*, 95:735, 1995.
[37] T.L. Thompson and J.T. Yates Jr. *Chem. Rev.*, 106:4428, 2006.
[38] R. Osgood. *Chem. Rev.*, 106:4379, 2006.

[39] M.-H. Du, J. Feng, and S.B. Zhang. *Phys. Rev. Lett.*, 98:066102, 2007.
[40] C. Gahl, K. Ishioka, Q. Zhong, Hotzel A, and M. Wolf. *Faraday Discuss.*, 117:191, 2000.
[41] H. Petek, H. Nagano, M. J. Weida, and S. Ogawa. *J. Phys. Chem. B*, 105:6767, 2001.
[42] G. Dutton, D.P. Quinn, C.D. Lindstrom, and X.-Y. Zhu. *Phys. Rev. B*, 72:045441, 2005.
[43] S. Ryu, J. Chang, H. Kwon, and S.K. Kim. *J. Vac. Sci. Techn. A*, 24:1454, 2006.
[44] A. Yang, S.T. Shipman, S. Garrett-Roe, J. Johns, M. Strader, P. Szymanski, E. Muller, and C. Harris. *J. Phys. Chem. C*, 112:2506, 2008.
[45] M.J. Comstock, N. Levy, A. Kirakosian, J.Cho, F. Lauterwasser, J.H. Harvey, D.A. Strubbe, J.M.J. Fréchet, D. Trauner, S.G. Louie, and M.F. Crommie. *Phys. Rev. Lett.*, 99:038301, 2007.
[46] C. Dri, M.V. Peters, J. Schwarz, S. Hecht, and L. Grill. *Nature Nanotech.*, 3:649, 2008.
[47] N. Levy, M.J. Comstock, J. Cho, L. Berbil-Bautista, A. Kirakosian, F. Lauterwasser, D.A. Poulsen, J.M.J. Fréchet, and M. F. Crommie. *Nano Lett.*, 9:935, 2009.
[48] G. Pace, V. Ferri, M. Elbing C. Grave, C. von Hänisch, M. Zharnikov, M. Mayor, M.A. Rampi, and P. Samorì. *PNAS*, 104:9937, 2007.
[49] V. Ferri, M. Elberg, G. Pace, M. Dickey, M. Zharnikov, P. Samori, M. Mayor, and M. Rampi. *Angew. Chem. Int. Ed.*, 47:3407, 2008.
[50] S. Yasuda, T. Nakamura, M. Matsumoto, and H. Shigekawa. *J. Am. Chem. Soc.*, 125:16430, 2003.
[51] A.S. Kumar, T. Ye, T. Takami, B.-C. Yu, A.K. Flatt, J.M. Tour, and P.S. Weiss. *Nano Lett.*, 8:1644, 2008.
[52] M. Ito, T.X. Wei, P.-L. Chen, H. Akiyama, M. Matsumoto, K. Tamada, and Y. Yamamoto. *J. Mater. Chem.*, 15:478, 2005.
[53] F. Callari, S. Petralia, and S. Sortino. *Chem. Commun.*, page 1009, 2006.
[54] M.J. Cook, A.-M. Nygård, Z. Wang, and D.A. Russell. *Chem. Commun.*, 22:1056, 2002.
[55] B. Baisch, D. Raffa, J. Lacour J. Kubitschke O.M. Magnussen, C. Nicolas, and R. Herges. *J. Am. Chem. Soc.*, 131:442, 2009.
[56] D. Bléger, A. Ciesielski, P. Samorì, and S. Hecht. *Chem. Eur. J.*, 16:14256, 2010.
[57] C. Gahl, R. Schmidt, D. Brete, W. Feyer E. McNellis, R. Carley, K. Reuter, and M. Weinelt. *J. Am. Chem. Soc.*, 132:1831, 2010.
[58] M. Utecht, t. Klamroth, and P. Saalfrank. *Phys. Chem. Chem. Phys.*, 13:21608, 2011.
[59] R. Klajn. *Pure Appl. Chem.*, 82:2247, 2010.
[60] D. Wang, Q. Chen, and L.-J. Wan. *Phys. Chem. Chem. Phys.*, 10:6467, 2008.
[61] S. Hagen, F. Leyssner, D. Nandi, M. Wolf, and P. Tegeder. *Chem. Phys. Lett.*, 444:85, 2007.
[62] L. Óvári, M. Wolf, and P. Tegeder. *J. Phys. Chem. C*, 111:15370, 2007.
[63] K. Morgenstern. *Prog. Surf. Sci.*, 86:115, 2011.
[64] B.-Y. Choi, S.-J. Kahng, S. Kim, H. Kim, H.W. Kim, Y.J. Song, J. Ihm, and Y. Kuk. *Phys. Rev. Lett.*, 96:156106, 2006.
[65] J. Henzl, M. Mehlhorn, H. Gawronski, K.-H. Rieder, and K. Morgenstern. *Angew. Chem. Int. Ed.*, 45:603, 2006.
[66] K. Morgenstern. *Acc. Chem. Res.*, 42:213, 2009.
[67] M. Alemani, M.V. Peters, S. Hecht, K.-H. Rieder, F. Moresco, and L. Grill. *J. Am. Chem. Soc.*, 128:14446, 2006.
[68] L. Grill. *J. Phys.: Condens. Matter*, 20:053001, 2008.
[69] N. Fuentes, A. Martin-Lasanta, L. Álvarez de Cienfuegos, M. Ribagorda, A. Parra, and J. M. Cuerva. *Nanoscale*, 3:4003, 2011.
[70] W.R. Browne and B.L. Feringa. *Nature Nanotech.*, 1:25, 2006.
[71] V. Balzani, A. Credi, and M. Venturi. *ChemPhysChem*, 9:202, 2008.
[72] M-M. Russew and S. Hecht. *Adv. Mater.*, 22:3348, 2010.
[73] D. Liu, Y. Xie, H. Shou, and X. Jiang. *Angew. Chem. Int. Ed.*, 48:4406, 2009.
[74] T Kawai, A. Sumi, C. Morita, and T. Kondo. *Colloids Surf. A*, 321:308, 2008.
[75] R. Klajn, P.J. Wesson, K.J.M. Bishop, and B.A. Grzybowski. *Angew. Chem. Int. Ed.*, 48:7035,

2009.
[76] X.-Y. Zhu. *Surf. Sci. Rep.*, 56:1, 2004.
[77] X.-Y. Zhu. *J. Phys. Chem. B*, 108:8778, 2004.
[78] J. Güdde, W. Berthold, and U. Höfer. *Chem. Rev.*, 106:4261, 2006.
[79] S. Sachs, C. H. Schwalb, M. Marks, A. Schll, F. Reinert, E. Umbach, and U. Höfer. *J. Chem. Phys.*, 131:144701, 2009.
[80] M. Winter, E. V. Chulkov, and U. Höfer. *Phys. Rev. Lett.*, 107:236801, 2011.
[81] M. Marks, N. L. Zaitsev, B. Schmidt, C. H. Schwalb, A. Schöll, I. A. Nechaev, P. M. Echenique, E. V. Chulkov, and U. Höfer. *Phys. Rev. B*, 84:081301, 2011.
[82] E. Varene, I. Martin, and P. Tegeder. *J. Phys. Chem. Lett.*, 2:252, 2011.
[83] E. Varene, L. Bogner, S. Meyer, Y. Pennec, and P. Tegeder. *Phys. Chem. Chem. Phys.*, 14:691, 2012.
[84] M. Weinelt. *J. Phys.: Condens. Matter*, 14:R1099, 2002.
[85] H. Ibach and D. Mills. *Electron energy loss spectroscopy and surface vibrations.* Academic Press, New York, 1982.
[86] Y.R. Shen. *The Principles of Nonlinear Optics.* Wiley, New York, 1984.
[87] Y.R. Shen. *Nature*, 337:519, 1989.
[88] T.F. Heinz. *Second-Order Nonlinear Optical Effects at Surfaces and Interfaces.* Elsevier, Amsterdam, 1991.
[89] M. Buck and M. Himmelhaus. *J. Vac. Sci. Technol. A*, 19:2717, 2001.
[90] M. A. Belkin and Y. R. Shen. *Int. Rev. Phys. Chem.*, 24:257, 2005.
[91] H.-F. Wang, W. Gan, R. Lu, Y. Rao, and B.-H. Wu. *Int. Rev. Phys. Chem.*, 24:191, 2005.
[92] M. Bonn, C. Hess, S. Funk, J.H. Miners, B.N.J. Persson, M. Wolf, and G. Ertl. *Phys. Rev. Lett.*, 84:4653, 2000.
[93] M. Yang and G.A. Somorjai. *J. Am. Chem. Soc.*, 126:7698, 2004.
[94] P. Galetto, H. Unterhalt, and G. Rupprechter. *Chem. Phys. Lett.*, 367:785, 2003.
[95] J.M. Gibbs-Davis, J.J. Kruk, C.T. Tonek, K.A. Scheidt, and F.M. Geiger. *J. Am. Chem. Soc.*, 130:15444, 2008.
[96] M. Sovago, R.K. Campen, G.W.H. Wurpel, M. Müller, H. J. Bakker, and M. Bonn. *Phys. Rev. Lett.*, 100:173901, 2008.
[97] H. Petek and S. Ogawa. *Prog. Surf. Sci.*, 56:239, 1997.
[98] H. Ibach. *Electron energy loss spectrometers.* Springer, Berlin, 1991.
[99] E.W. Plummer and W. Eberhardt. *Adv. Chem. Phys.*, 49:533, 1985.
[100] P.J. Benning, D.M. Poirier, T.R. Ohno, Y. Shen, F. Stepniak M.B. Jost, G.H. Kroll, J.H. Weaver, J. Fure, and R.E. Smalley. *Phys. Rev. B*, 45:6899, 1992.
[101] S. Hagen, Y. Luo, R. Haag, M. Wolf, and P. Tegeder. *New J. Phys.*, 12:125022, 2010.
[102] Y.J. Chabal. *Surf. Sci. Rep.*, 8:211, 1988.
[103] F.M. Hoffmann. *Surf. Sci. Rep.*, 3:107, 1983.
[104] S. Funk, M. Bonn, D.N. Denzler, Ch. Hess, M. Wolf, and G. Ertl. *J. Chem. Phys.*, 112:9888, 2000.
[105] S. Hagen, P. Kate, M.V. Peters, S. Hecht, M. Wolf, and P. Tegeder. *Appl. Phys. A*, 93:253, 2008.
[106] S. Hagen, P. Kate, F. Leyssner, D. Nandi, M. Wolf, and P. Tegeder. *J. Chem. Phys.*, 129:164102, 2008.
[107] M. Wolf and P. Tegeder. *Surf. Sci.*, 603:1506, 2009.
[108] J. Mielke, F. Leyssner, M.s Koch, S. Meyer, Y. Luo, S. Selvanathan, R. Haag, P. Tegeder, and L. Grill. *ACS Nano*, 5:2090, 2011.
[109] F. Leyssner, S. Hagen, L. Óvári, J. Dokic, P. Saalfrank, M. V. Peters, S. Hecht, T. Klamroth, and P. Tegeder. *J. Phys. Chem. C*, 114:1231, 2010.
[110] L. Óvári, J. Schwarz, M.V. Peters, S. Hecht, M. Wolf, and P. Tegeder. *Int. J. Mass. Spectrom.*, 277:223, 2008.
[111] P. Tegeder, S. Hagen, F. Leyssner, M.V. Peters, S. Hecht, T. Klamroth, P. Saalfrank, and M. Wolf.

Appl. Phys. A, 88:465, 2007.
[112] A. Kirakosian, M.J. Comstock, Jongweon Cho, and M.F. Crommie. *Phys. Rev. B*, 71:113409, 2005.
[113] J.A. Miwa, S. Weigelt, H. Gersen, F. Besenbacher, F. Rosei, and T.R. Linderoth. *J. Am. Chem. Soc.*, 128:3164, 2006.
[114] N. Henningsen, K.J. Franke, G. Schulze, I. Fernández-Torrente, B. Prietwisch, K. Rück-Braun, and J.I. Pascual. *Chem. Phys. Chem.*, 9:71, 2008.
[115] Y. Wang, X. Ge, G. Schull, R. Berndt, C. Bornholdt, F. Koehler, and R. Herges. *J. Am. Chem. Soc.*, 103:4218, 2008.
[116] M. Alemani, S. Selvanathan, F. Ample, K.-H. Rieder M. V. Peters, F. Moresco, Ch. Joachim, S. Hecht, and L. Grill. *J. Phys. Chem. C*, 112:10509, 2008.
[117] S. Selvanathan, M.V. Peters, J. Schwarz, S. Hecht, and L. Grill. *Appl. Phys. A*, 93:247, 2008.
[118] M.J. Comstock, J. Cho, A. Kirakosian, and M.F. Crommie. *Phys. Rev. B*, 72:153414, 2005.
[119] N. Henningsen, K. J. Franke, I. F. Torrente, G. Schulze, B. Priewisch, K. Rück-Braun, J. Dokić, T. Klamroth, P. Saalfrank, and J. I. Pascual. *J. Phys. Chem. C*, 111:14843, 2007.
[120] J. Henzl, T. Bredow, and K. Morgenstern. *Chem. Phys. Lett.*, 435:278, 2007.
[121] J. Henzl, M. Mehlhorn, and K. Morgenstern. *Nanotechnology*, 18:495502, 2007.
[122] N. Henningsen, R. Rurali, K.J. Franke, I. Fernández-Torrente, and J.I. Pascual. *Appl. Phys. A*, 93:241, 2008.
[123] M.J. Comstock, N. Levy, J. Cho, L. Berbil-Bautista, M.F. Crommie, D.A. Poulsen, and J.M.J. Fréchet. *Appl. Phys. Lett.*, 92:123107, 2008.
[124] R. Schmidt, S. Hagen, D. Brete, R. Carley, C. Gahl, J. Dokic, P. Saalfrank, S. Hecht, P. Tegeder, and M. Weinelt. *Phys. Chem. Chem. Phys.*, 12:4488, 2010.
[125] E. R. McNellis, C. Bronner, J. Meyer, M. Weinelt, P. Tegeder, and K. Reuter. *Phys. Chem. Chem. Phys.*, 12:6404, 2010.
[126] M. Rohleder, W. Berthold, J. Güdde, and U. Höfer. *Phys. Rev. Lett.*, 94:017401, 2005.
[127] W. Berthold, F. Rebentrost, P. Feulner, and U. Höfer. *Appl. Phys. A*, 78:131, 2004.
[128] M. Rohleder, K. Dunker, W. Berthold, J. Güdde, and U. Höfer. *New J. Phys.*, 7:103, 2005.
[129] M. Muntwiler, C.D. Lindstrom, and X.-Y. Zhu. *J. Chem. Phys.*, 124:81104–1, 2006.
[130] C. Bronner, M. Schulze, S. Hagen, and P. Tegeder. *New J. Phys.*, submitted, 2012.
[131] H. Eckhart, L. Fritsche, and J. Noffke. *J. Phys. F: Met. Phys.*, 14:97, 1984.
[132] R. Courths, H.-G. Zimmer, A. Goldmann, and H. Saalfeld. *Phys. Rev. B*, 34:3577, 1986.
[133] F. Reinert, G. Nicolay, S. Schmidt, D. Ehm, and S. Hüfner. *Phys. Rev. B*, 63:115415, 2001.
[134] C.D. Lindstrom, D. Quinn, and X.-Y. Zhu. *J. Chem. Phys.*, 122:124714, 2005.
[135] T. Fauster and W. Steinmann. *Electromagnetic Waves: Recent Developments in Research.* Elsevier, Amsterdam, 1995.
[136] U. Thomann M. Kutschera M. Weinelt T. Fauster U. Höfer C. Reuß, I. L. Shumay. *Phys. Rev. Lett.*, 82:153, 1999.
[137] W. Berthold, F. Rebentrost, P. Feulner, and U. Höfer. *Appl. Phys. A.*, 78:131, 2004.
[138] K. Boger, M. Weinelt, and T. Fauster. *Phys. Rev. Lett.*, 92:126803, 2004.
[139] P. Tegeder, M. Danckwerts, S. Hagen, A. Hotzel, and M. Wolf. *Surf. Sci.*, 585:177, 2005.
[140] G. Füchsel, T. Klamroth, J. Dokić, and P. Saalfrank. *J. Phys. Chem. B*, 110:16337, 2006.
[141] R. Kübler, W. Lüttke, and S. Weckherlin. *Z. Elektrochem.*, 64:650, 1960.
[142] B. Kellerer, H.H. Hacker, and J. Brandmüller. *Ind. J. Pure Appl. Phys.*, 9:903, 1971.
[143] S. Hagen. *Isomerization behavior of photochromic molecules in direct contact with noble metal surfaces.* PhD thesis; Freie Universität Berlin, 2009.
[144] P. Tegeder, F. Brüning, and E. Illenberger. *Chem. Phys. Lett.*, 310:79, 1999.
[145] F. Brüning, P. Tegeder, J. Langer, and E. Illenberger. *Int. J. Mass Spectrom.*, 195:507, 2000.
[146] E. Knoesel, A. Hotzel, and M. Wolf. *Phys. Rev. B*, 57:12812, 1998.
[147] H. Petek, H. Nagano, and S. Ogawa. *Phys. Rev. Lett.*, 83:832, 1999.
[148] H. Petek, H. Nagano, and S. Ogawa. *Appl. Phys. B*, 68:369, 1999.

[149] R. Matzdorf, A. Gerlach, F. Theilmann, G. Meister, and A. Goldmann. *Appl. Phys. B*, 68:393, 1999.
[150] J.A. Misewich, S. Nakabayashi, P. Weigand, M. Wolf, and T.F. Heinz. *Surf. Sci.*, 363:204, 1996.
[151] S. Weigelt, C. Busse, L. Petersen, E. Rauls, B. Hammer, K.V. Gothelf, F. Besenbacher, and T.R. Linderoth. *Nature Mat.*, 5:112, 2006.
[152] J. Dokić, M. Gothe, J. Wirth, M.V. Peters, J. Schwarz, S. Hecht, and P. Saalfrank. *J. Phys. Chem. A*, 113:6763, 2009.
[153] L. Óvári, Y. Luo, F. Leyssner, R. Haag, M. Wolf, and P. Tegeder. *J. Chem. Phys.*, 133:044707, 2010.
[154] E.R. McNellis, G. Mercurio, S. Hagen, F. Leyssner, J. Meyer, S. Soubatch, M. Wolf, K. Reuter, P. Tegeder, and F.S. Tautz. *Chem. Phys. Lett.*, 499:247, 2010.
[155] G. Mercurio, E. McNellis, I. Martin, S. Hagen, F. Leyssner, S. Soubatch, J. Meyer, M. Wolf, P. Tegeder, F.S. Tautz, and K. Reuter. *Phys. Rev. Lett.*, 104:036102, 2010.
[156] J. Zegenhagen. *Surf. Sci. Rep.*, 18:199, 1993.
[157] D.P. Woodruff. *Prog. Surf. Sci.*, 57:1, 1998.
[158] D.P. Woodruff. *Prog. Phys.*, 68:743, 2005.
[159] A. Padwa. *Chem. Rev.*, 77:1, 1977.
[160] E. Haselbach and E. Heilbronner. *Helv. Chim. Acta*, 16:16, 1968.
[161] L.N. Patnaik and S. Das. *Int. J. Quantum Chem.*, 27:135, 1985.
[162] A.V. Gaenko, A. Devarajan, L. Gagliardi, R. Lindh, and G. Orlandi. *Theor. Chem. Acc.*, 118:271, 2007.
[163] J.W. Lewis and C. Sandorty. *Can. J. Chem.*, 90:1738, 1982.
[164] M. Piantek, G. Schulze, M. Koch, K.J. Franke, F. Leyssner, A. Krüger, C. Navío, J. Miguel, M. Bernien, M. Wolf, W. Kuch, P. Tegeder, and J.I. Pascual. *J. Am. Chem. Soc.*, 131:12729, 2009.
[165] J. P. Collman, L.S. Hegedus, J.R. Norton, and R.G. Finke, editors. *Principles and Applications of Organotransition Metal Chemistry*. University Science Books: Mill Valley, CA, 1987.
[166] R. Cortés, A. Mascaraque, P. Schmidt-Weber, H. Dil, T.U. Kampen, and K. Horn. *Nano Lett.*, 8:4162, 2008.
[167] P.M. Schmidt, K. Horn, J.H. Dil, and T.U. Kampen. *Surf. Sci.*, 601:1775, 2007.
[168] C.-S. Tsai, J.-K. Wang C. Su, and C.-J. Lin. *Langmuir*, 19:822, 2003.
[169] L.-W. Chou, Y.-R. Lee, C.-M. Wei, J.-C. Jiang, J.-C. Lin, and J.-K. Wang. *J. Phys. Chem. C*, 113:208, 2009.
[170] C.-S. Tsai, J.-K. Wang, R.T. Skodje, and J.-C. Lin. *J. Am. Chem. Soc.*, 127:10788, 2005.
[171] R.M. Slayton, N.R. Franklin, and N.J. Tro. *J. Phys. Chem.*, 100:15554, 1996.
[172] M.V. Peters. *PhD-thesis, Humboldt Universität Berlin*, 2008.
[173] G. Cottone, R. Noto, and G. La Manna. *Chem. Phys. Lett.*, 388:218, 2004.
[174] H. Görner. *Phys. Chem. Chem. Phys.*, 3:416, 2001.
[175] J. T .C. Wojtyk, P. M. Kazmaierb, and E. Buncel. *Chem. Comm.*, page 1703, 1998.
[176] R.J. Byrne, S.E. Stitzel, and D. Diamond. *J. Mat.*, 16:1332, 2006.
[177] T. Huang, Z. Hu, A. Zhao, H. Wang, B. Wang, J. Yang, and J. G. Huo. *J. Am. Chem. Soc.*, 129:14843, 2007.
[178] T. Huang, Z. Hu, B. Wang, L. Chen, A. Zhao, H. Wang, and J. G. Huo. *J. Phys. Chem. B*, 111:6973, 2007.
[179] M. Karcher, C. Rüdt, C. Elsäßer, and P. Fumagalli. *J. Appl. Phys.*, 102:084904, 2007.
[180] A. E. Baber, S. C. Jensen, E. V. Iski, and E. C. H. Sykes. *J. Am. Chem. Soc.*, 129:6368, 2007.
[181] T. Yokoyama, T. Takahashi, K. Shinozaki, and M. Okamoto. *Phys. Rev. Lett.*, 98:206102, 2007.
[182] I.F. Torrente, S. Monturet, K. J. Franke, J. Fraxedas, N. Lorente, and J.I. Pascual. *Phys. Rev. Lett.*, 99:176103, 2007.
[183] C. Bronner, G. Schulze, K. J. Franke, J. I. Pascual, and P. Tegeder. *J. Phys.: Condens. Matter*, 23:484005, 2011.

[184] H. Jian and J.M. Tour. *J. Org. Chem.*, 68:5091, 2003.
[185] Y. Shirai, L. Cheng, B. Cheng, and J.M. Tour. *J. Am. Chem. Soc.*, 128:13479, 2006.
[186] E. Galoppini, W. Guo, W. Zhang, P.G. Hoertz, P. Qu, and G.J. Meyer. *J. Am. Chem. Soc.*, 124:7801, 2002.
[187] D. Takamatsu, Y. Yamakoshi, and K. Fukui. *J. Phys. Chem. B*, 110:1968, 2006.
[188] S. Wagner, F. Leyssner, C. Kördel, S. Zarwell, R. Schmidt, M. Weinelt, K. Rück-Braun, M. Wolf, and P. Tegeder. *Phys. Chem. Chem. Phys.*, 11:6242, 2009.
[189] S. Zarwell and K. Rück-Braun. *Tetrahedron Lett.*, 49:4020, 2008.
[190] A.J. Heinrich, C.P. Lutz, J.A. Gupta, and D.M. Eigler. *Science*, 297:1853, 2002.